

Review

Structure, Properties, and Reactivity of Porphyrins on Surfaces and Nanostructures with Periodic DFT Calculations

Bhaskar Chilukuri *, Ursula Mazur and K. W. Hipps

Department of Chemistry, Washington State University, Pullman, WA 99163-4630, USA;
umazur@wsu.edu (U.M.); hipps@wsu.edu (K.W.H.)

* Correspondence: bhaskar.chilukuri@wsu.edu

Received: 30 December 2019; Accepted: 17 January 2020; Published: 21 January 2020



Featured Application: Choosing appropriate DFT methodology for periodic modeling of porphyrin containing systems.

Abstract: Porphyrins are fascinating molecules with applications spanning various scientific fields. In this review we present the use of periodic density functional theory (PDFT) calculations to study the structure, electronic properties, and reactivity of porphyrins on ordered two dimensional surfaces and in the formation of nanostructures. The focus of the review is to describe the application of PDFT calculations for bridging the gaps in experimental studies on porphyrin nanostructures and self-assembly on 2D surfaces. A survey of different DFT functionals used to study the porphyrin-based system as well as their advantages and disadvantages in studying these systems is presented.

Keywords: porphyrins; density functional theory; DFT; surfaces; self-assembly; scanning tunneling microscopy; dispersion; nanostructures; solid state; condensed phase

1. Introduction

Porphyrins are tetrapyrrolic macrocycles with π -conjugated electronic system that are ubiquitous in nature and have numerous biological and technological applications. For example, porphyrins are found in our body as prosthetic groups in hemoproteins. In plants, porphyrins are important components of chlorophyll which is a pigment playing an essential role in photosynthesis. Porphyrins also have numerous biomedical applications including photoimmunotherapy, photo diagnosis [1], biosensors [2], cancer therapy, etc. Porphyrins also play an important role in organic synthesis of dendrimers [3], metal-organic frameworks (MOFs) [4], biomimetic reactions [5], and as photo-catalysts [6] in numerous oxidation/reduction reactions. Finally, porphyrins act as important components in various technological applications like solar cells [7], chemical sensors [8], optoelectronics [9], spintronics [10], field effect transistors (FETs) [11–14], and in nanotechnology like single molecule junctions [15], nanowires, nanomotors [10], etc.

All the applications listed above are possible only due to the characteristic, yet tunable chemical structure and properties of porphyrins [16]. The backbone of each porphyrin molecule is the porphine group which constitutes four pyrrole groups linked with methine (-CH-) bridges, Figure 1a. Each porphine group has 22 π electrons forming a conjugated system. Due to their large pi-conjugation, porphyrins have strong absorption in the UV and visible regions forming colored compounds. In addition, the large π -electron system is responsible for many properties of porphyrins including optical [17,18], electronic [19], mechanical [20], and chemical [21,22] properties. Additionally, porphyrins form many coordinate covalent complexes with transition metals (metalloporphyrins) and

some non-metals at the center of the porphyrin core. In addition, the peripheral substituents at α , β , and meso positions (Figure 1b) can be modified to yield tunable molecular and crystal properties such as solubility, reactivity, conductivity, and photophysics. Metalloporphyrins tend to react with ligands to form numerous (porphyrin)metal-ligand complexes [23] that are also useful for a variety of applications.

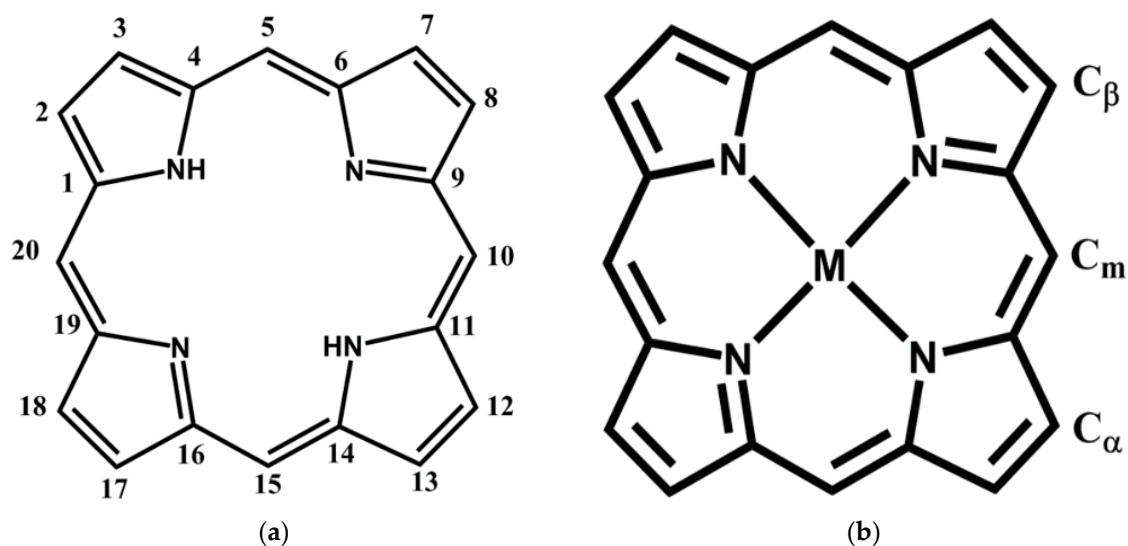


Figure 1. Chemical structures of (a) freebase porphine/porphyrin, (b) metalloporphyrin. Three unique peripheral substituent positions, alpha (C_α) at 2, 7, 12, 18; beta (C_β) at 3, 8, 13, 18; and meso (C_m) at 5, 10, 15, 20 positions are shown the figure.

A broad scan of the literature of theoretical modeling of porphyrins showed that a variety of computational methods were used to study porphyrins and their derivatives. A review by Shubina [24] listed these computational methods, which ranged from linear combination of atomic orbitals (LCAO), molecular mechanics, semi-empirical methods, through self-consistent field method (SCF) in the earlier literature, to the modern day methods which include molecular dynamics (MD), density functional theory (DFT) [25], Moller-Plesset perturbation theory (MPn), configuration interaction (CI), coupled cluster (CC), and CASSCF/CASPT2 [26] methods. Among the many computational methods used, recent literature is flooded with DFT calculations of molecular porphyrin and its derivatives primarily to understand their frontier orbital configuration, electron occupancy [27], charge transfer, and excited state properties [25]. The DFT functionals used to study the porphyrin complexes include all the rungs of the “Jacob’s Ladder” [28] with variable approximations which include local density approximation (LDA), generalized gradient approximations (GGA), meta-GGAs, hybrid, and hybrid-meta GGA functionals [29,30].

While molecular DFT calculations of porphyrin complexes are prevalent, periodic DFT calculations of porphyrins are relatively limited. Periodic DFT (PDFT) calculations [31] refers to the use of density functional theory to describe the electronic structure of periodic systems. PDFT simulations are performed on lattice structures, surfaces, interfaces, and molecules with a defined unit cell in real and reciprocal spaces (k-space). The reciprocal space is obtained from the Brillouin zone of the unit cell. A grid of k-points is used to sample the Brillouin zone by using Bloch’s theorem applied to the Kohn-Sham wavefunctions. Optimization and single point calculations with PDFT are performed using various self-consistent field (SCF) iteration schemes. While Gaussian basis sets can be used to perform PDFT calculations, plane wave pseudopotential basis sets are computationally less intensive and are used in many PDFT codes [32].

In this review we present a collection of DFT simulations of periodic systems containing porphyrins. While we tried to include many PDFT studies of porphyrins in this review, these are not necessarily a

complete collection in the literature. Omission of a particular citation is not a reflection on the quality of that work.

Periodic DFT calculations of porphyrins can be broadly classified into two categories. First, simulation of porphyrin crystals, supramolecular compounds, and nanostructures like nanorods, nanowires, and nanosheets. Typical interests for these simulations involve understanding the intermolecular or packing interactions of porphyrins and determining their electronic properties, specifically band structure and density of states. The second category involves porphyrin interactions with solid supports like metals, oxides, carbon, and silicon surfaces. PDFT simulations on surfaces typically involve a molecule or monolayer of porphyrins or metalloporphyrins adsorbed on solid supports to study the adsorption configuration, binding energies, molecule-surface interactions and reactions, electronic structure using density of states (DOS) and band structure, chemical reactivity, interfacial charge distribution, and magnetic properties. Some of the *ab initio* DFT codes used for porphyrin PDFT simulations include VASP [33–35], Quantum Espresso [36], CP2K [37], CASTEP [38], Dmol [39], SIESTA [40], CPMD [41], etc. Omission of any code is not a reflection of the quality of the software for PDFT simulations. However, we note that codes involving plane-wave basis sets are more popular than software that are based on Gaussian type orbital (GTO) and natural atomic orbital (NAO) basis sets.

2. PDFT Simulations of Porphyrins in Nanostructures

Due to their rich chemistry, porphyrins can be synthesized through chemical bonding or through self-assembly into multiple structural forms like crystals, needles, wires, rods, sheets, plates, supramolecular frameworks, tubes, spheres, etc. PDFT simulations of these porphyrin structures primarily involves studying the stacking and intermolecular interactions inside a given geometry and their relation to its material properties. PDFT simulations of porphyrin nanostructures in the bulk were performed either from an experimental crystal structure or a built model based on experimental data and molecular structure. Most of these simulations aim to determine the electronic band structure and density of states. In the following sections we have classified the PDFT simulations on the porphyrin nanostructures based on their shape in the periodic structure.

2.1. Porphyrin Nanostructures Using Crystal Geometries

There are many known single crystal structures of porphyrins and metalloporphyrins in the literature but PDFT simulations on lattice structures of porphyrins are seldom found. Single crystal structures from x-ray crystallography of porphyrin nanostructures are even rare. Adinehnia et al. [42] determined the first single crystal structure of ionic porphyrin nanorods involving meso-tetra(N-methyl-4-pyridyl)porphyrin (TMPyP) and meso-tetra(4-sulfonatophenyl)porphyrin (TSPP). Using various spectroscopic, diffraction, and imaging techniques, they reported the structure-function relationship of TMPyP:TSPP nanorods. The crystal structure was correlated to the morphology and photoconductive behavior of the nanorods, and PDFT calculations on the crystal structure showed that the π - π stacking of TMPyP:TSPP is responsible for their conductivity.

Figure 2 shows the crystal structure and the corresponding band structure of TMPyP:TSPP nanorods. The band structure was determined using optB88-van der Waals (vdW) GGA [43] functional with projector augmented wave (PAW) [35,44] Perdew-Burke-Ernzerhof (PBE) [45] pseudopotentials. The authors note that the band structure obtained with PDFT underestimates the band gap (0.90 eV) and extended Huckel tight binding (EHTB) was used to determine the band gap (1.3 eV) which matches closer to experiment. Hybrid DFT functionals such as Heyd-Scuseria-Ernzerhof (HSE) [46,47] have shown improved band gap prediction over GGA and LDA functionals. Although HSE can improve band gap prediction, geometric optimizations showed little change in contrast to GGA and LDA functionals. On the other hand, vdW-DF [43,48] functionals were more reliable for geometric optimizations in systems with considerable dispersion interactions.

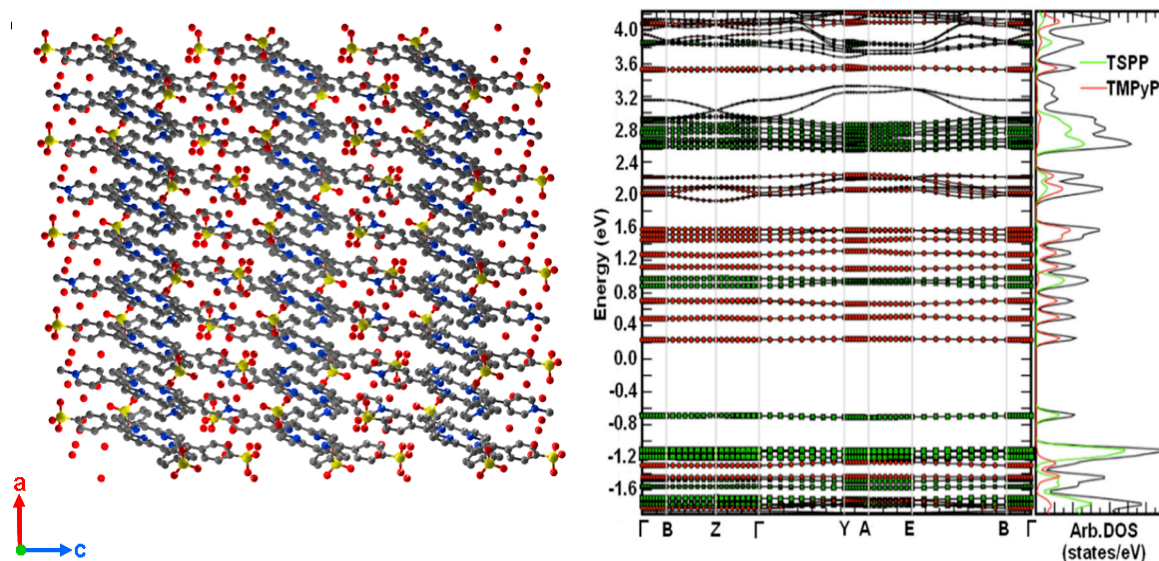


Figure 2. On the left, crystal structure of meso-tetra(N-methyl-4-pyridyl)porphyrin (TMPyP):meso-tetra(4-sulfonatophenyl)porphyrin (TSPP) nanorods in direction normal to the crystallographic b axis, showing the alternating cationic and anionic porphyrin tectons within the columns. Color codes: blue, N; gray, C; yellow, S; red, O. On the right is the projected density of states and band structure for the TMPyP:TSPP crystal computed from periodic density functional theory (PDFT). The Fermi level (E_f) is set as zero. The high symmetry points the Brillouin zone are as follows, $G = (0,0,0)$, $Z = (0,0,0.5)$, $Y = (0,0.5,0)$, $X = (0.5,0,0)$, $A = (-0.5,0,0.5)$, $E = (-0.5,0.5,0.5)$, $B = (0,0,0.5)$. Reproduced from reference [42] published by The Royal Society of Chemistry.

In the case of TMPyP:TSPP, DFT calculations have been useful to predict the appropriate partial density of states (pDOS) that showed that the top of the valence band is populated by the contributions from TSPP and the bottom of the conduction band is populated by the TMPyP with no orbital hybridization in the vicinity of the bandgap. This prediction was consistent with the experimental data from UV-visible, diffuse reflectance and photoconductivity action spectra. This shows that PDFT calculations played a critical role in elucidating the photoconductive mechanism in TMPyP:TSPP nanorods. In the same study the authors reported that decreasing the porphyrin stacking distance would not necessarily change the band gap but would increase the dispersion in the band structure which would improve charge mobility in the nanorods.

The work on TMPyP:TSPP nanorods has been expanded by Borders et al. [49], by selective metalation of TMPyP and TSPP porphyrin cores with Ni and Cu transition metals. A single crystal structure of H_2 TMPyP:NiTSPP nanorods was determined and it was shown that metalation of ionic porphyrins led to exhibition of dark conductivity at moderately high temperatures and that conductivity increases upon photoexcitation. Additionally, the photoresponse of the H_2 TMPyP:CuTSPP substituted crystals is significantly higher than that of the CuTMPyP: H_2 TSPP and the Ni-substituted crystals. To understand the reasons behind this discrepancy in the conductive behavior with different metalation, PDFT calculations were performed on H_2 TMPyP:(M)TSPP and (M)TMPyP: H_2 TSPP systems, where $M = Ni, Cu$. The crystal structure of H_2 TMPyP:NiTSPP was used to create the lattice structure of other metalated binary ionic porphyrins by changing the core substitution of the H_2 TMPyP:NiTSPP crystals and then optimizing the structure. The band structure of each H_2 TMPyP:(M)TSPP and (M)TMPyP: H_2 TSPP systems are shown in Figure 3. It was reported that adding a metal to the freebase porphyrins reduces the band gap of the corresponding nanorods. Additionally, it was shown that Ni and Cu metalation causes distinct changes in the frontier bands of porphyrin nanostructures.

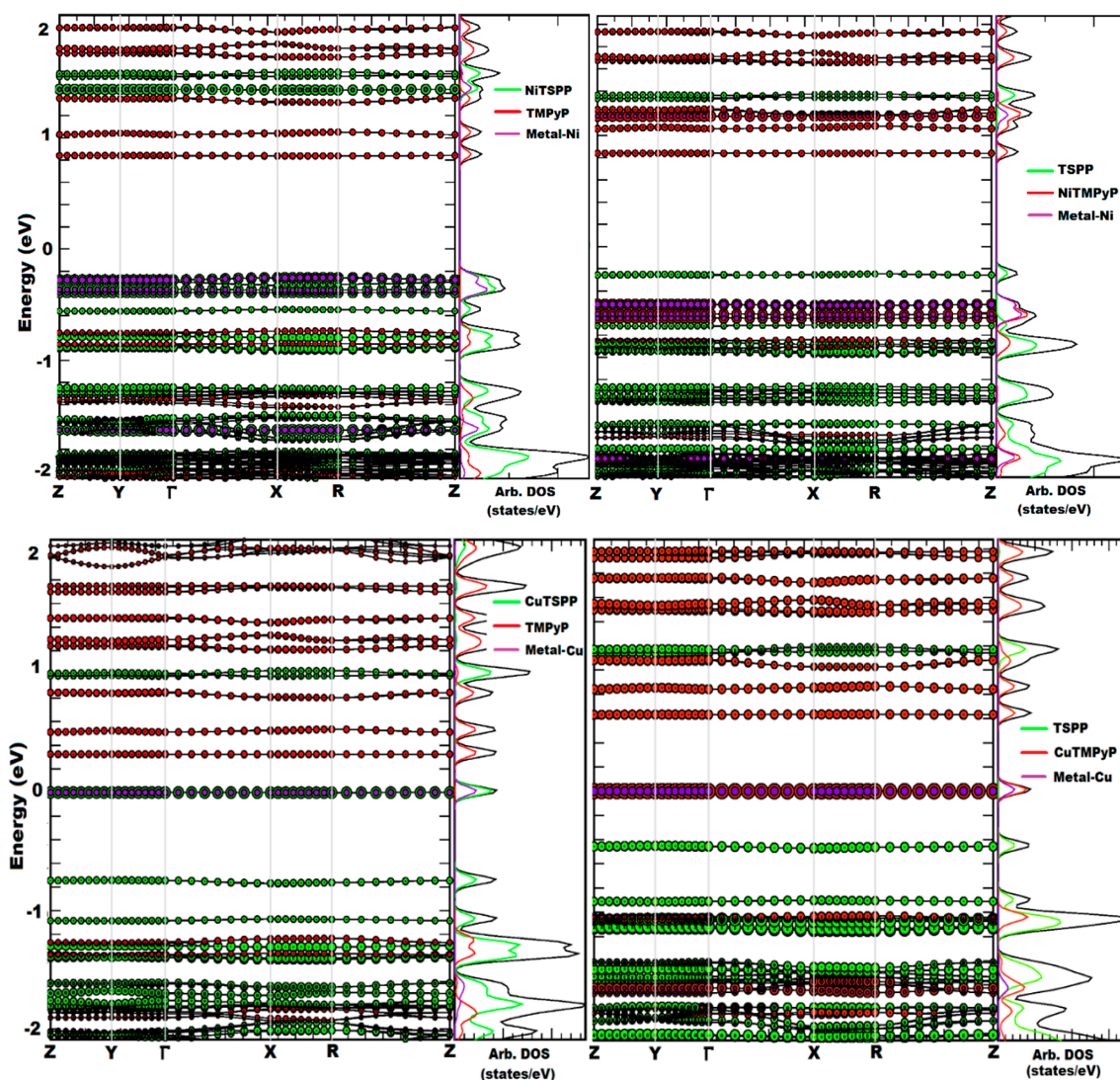


Figure 3. Projected density of states and the band structure for the H_2 TMPyP:NiTSPP, NiTMPyP: H_2 TSPP, H_2 TMPyP:CuTSPP, and CuTMPyP: H_2 TSPP crystals computed from DFT. The Fermi level (E_f) is set at zero. The high symmetry points of the Brillouin zone are as follows, $G = (0,0,0)$, $Z = (0,0,0.5)$, $Y = (0,0.5,0)$, $X = (0.5,0,0)$, and $R = (0.5,0.5,0.5)$. Reproduced from reference [49] published by The Royal Society of Chemistry.

As mentioned earlier, PDFDT studies of x-ray crystal structures of porphyrins are rare. Some of the other studies include determination of surface free energy of different crystal faces of FeTPPCL (TPP = tetra-phenyl porphyrin) and FeTPPOH· H_2O nanocrystals by Tian et al. [50]. They used PDFDT calculated surface energies of {001}, {100}, {110}, {011} crystal faces to understand and tune the growth and shape of the FeTPP based nanocrystals. The calculations were performed using GGA-PBE [45] functional on predetermined crystal structures of FeTPPCL and FeTPPOH· H_2O from the Cambridge Crystallographic Data Centre (CCDC) database. Krasnov et al. [51] performed a PDFDT study of porphyrin:fullerene supramolecular compounds using models constructed from x-ray crystal structures determined by Boyd et al. [52]. The PBE functional [45] with Grimme DFT-D2 [53] dispersion interaction correction was used to optimize the models of porphyrin:fullerene compounds. The band structure and absorbance spectra of various optimized structures were determined using HSE [47] functional and DFPT [54] method, respectively. The HSE functional is a hybrid functional used for improved band gap prediction.

2.2. Porphyrins in Organic Frameworks

Porphyrins are used to develop many supramolecular frameworks like metal organic (MOF), covalent organic (COF), surface metal organic (SURMOF) frameworks with applications for gas storage/separation, catalysis, drug delivery, photovoltaics, etc. Hence, PDFT calculations of porphyrin organic frameworks have gained importance for understanding their electronic structure to tune their applications. Hamad et al. [55], studied the electronic structure of porphyrin-based MOFs (PMOF) with porphyrins connected through phenyl-carboxyl ligands and AlOH species to assess their suitability for the photocatalysis of fuel production reactions using sunlight. They used the rhombohedral primitive cell obtained from the orthorhombic crystal structure of Al-PMOF [56] and replaced the porphyrin core with either hydrogens or various 3d transition metals and performed PDFT calculations of each model. The calculations were performed with GGA-PBE [45] functional starting with optimization of each lattice structure, followed by single point calculations for determination of DOS and band structure with HSE06 functional [46,47]. A typical crystal structure of the PMOF unit cell is presented in Figure 4a. From PDFT calculations, they reported that the bandgaps for PMOFs are in a favorable range (2.0–2.6 eV) for efficient adsorption of solar light. Furthermore, it was shown that the MOFs' band edges align with the redox potentials (Figure 4b) for water splitting and carbon dioxide reduction with reactions that can occur at neutral pH. This study was followed up with another PDFT study by Aziz et al. [4] by modifying the octahedral Aluminum metal center of the lattice structure with Fe^{+3} metal to determine the changes in the band structure and electronic properties of PMOFs. It was reported that adding Fe at the porphyrin core slightly raises the valence band edge, while Fe at the octahedral node significantly lowers the conduction band edge. So, iron can be used as a good dopant for band structure alignment in porphyrin-based MOFs.

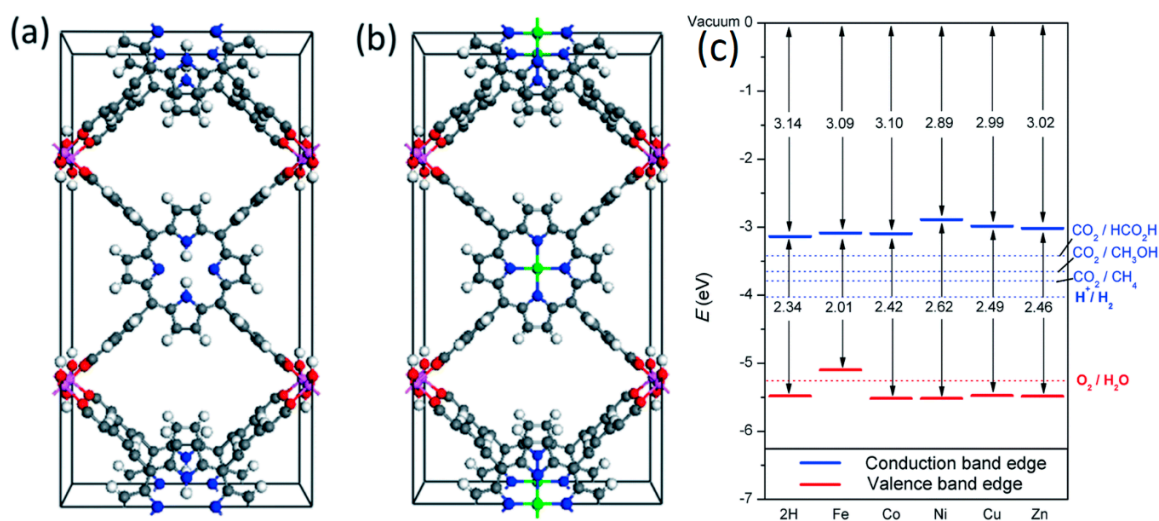


Figure 4. Perspective view of the porphyrin-based metal organic framework (MOF) investigated in this study in (a) the protonated case, and (b) the metal-substituted case. Color code: gray = carbon, white = hydrogen, red = oxygen, blue = nitrogen, magenta = aluminum, green = transition metal. (c) Bandgaps and band edge positions of MOFs with respect to the vacuum level, as calculated with the HSE06 functional. Energy levels corresponding to redox potentials of water splitting and carbon dioxide reduction reactions producing methane, methanol, and formic acid at pH = 7 are also shown with dotted lines. Reproduced from reference [55] published by The Royal Society of Chemistry.

PDFT calculations of porphyrin based SURMOFs has been reported by Liu et al. [57,58], who studied the photophysical properties of Zn(II)porphyrin-based SURMOFs. Using PDFT band structure with PBE functional [45] it was shown that a small dispersion of occupied and unoccupied bands in the Γ -Z direction [57], which is the porphyrin stacking direction, leads to the formation of a small indirect band gap. In a follow up study [58], the effect of introducing an electron-donating diphenylamine (DPA)

into Zn SURMOFs was studied and PDFT simulations showed that DPA causes a shift in the charge localization pattern in the valence band minimum. This charge shift was attributed to the DPA groups which causes a shift of the optical absorption spectrum and the improved photocurrent generation in Zn SURMOFs. PDFT simulations are also used to study the stability of the porphyrin-COFs upon gas adsorption. Ghosh et al. used GGA-PW91 [59] and LDA-PZ [60] functionals to study hydrogen storage in H₂P-COF. The structural stability of COF upon introducing pyridine molecules to bridge the interlayer gaps in porphyrin COFs is studied.

2.3. Porphyrins as Nano Wires, Sheets, Tubes, and Ladders

As mentioned earlier, porphyrins can form many structural shapes due to their mechanical flexibility and rich chemistry. Hence, PDFT simulations were used to study the unique electronic structures and their applications that are possible because of the multidimensionality of porphyrins. Figure 5 shows typical shapes—various porphyrin nanowires, nanotubes, and nanosheets. Posligua et al. [61] studied the band structures of porphyrin nano sheets and tubes formed through covalent linkers. They used screened hybrid density functional theory simulations and Wannier function interpolation to obtain accurate band structures. The structural optimizations were performed with PBE-D2 [45,53] functional and single point calculations for band structure were obtained using the HSE06 [46,47] functional. It was reported that the electronic properties exhibit strong variations with the number of linking carbon atoms (C0 = no carbon atoms, C2 = two carbon atoms, C4 = four carbon atoms). For example, all C0 nanostructures exhibit gapless or metallic band structures, whereas band gaps open for the C2 or C4 structures. PDFT simulations showed that it is possible to design porphyrin nanostructures with tailored electronic properties such as specific band gap values and band structures by varying the type of the linkage used between each porphyrin units and the type of self-assembled formations (linear chains, nanosheets, nanotubes, and nanorings). A previous study on porphyrin nanotubes formed with acetyl linkers was done by Allec et al. [62] who reported large oscillations in bandgaps of porphyrin nanotubes with increase in their size. The simulations were performed with a variety of periodic DFT functionals which show similar oscillation trend in the band gaps irrespective of the functional. Additionally, the authors report that the bandgap is a direct-bandgap which can be observed with photoelectron spectroscopic experiments.

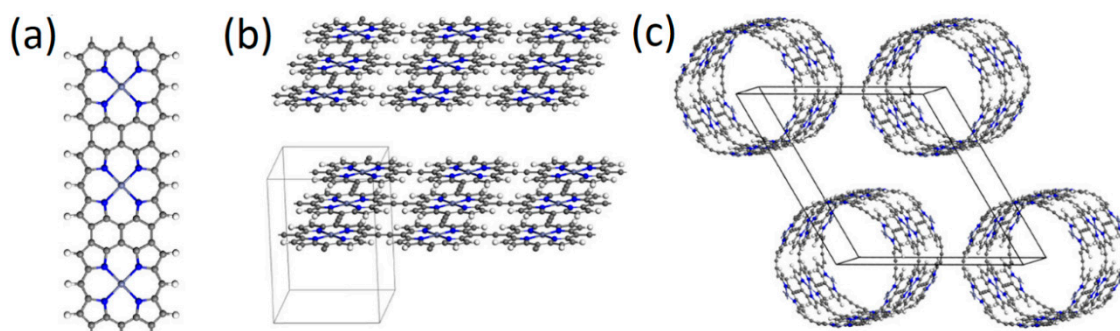


Figure 5. Typical structures of porphyrin (a) nanowire, (b) nanosheets, and (c) nanotubes. Reprinted with permission from reference [61] Copyright 2018 American Chemical Society.

Various porphyrin nanosheet structures with variable porphyrin core metals and substituents were also studied extensively with PDFT calculations. Using the GGA-PBE functional [45], Singh et al. [63] predicted the stable formation of a 2D ferromagnetic half-metal based on vanadium polyporphyrin (PP). The stability of the 2D metal was determined by comparing the Curie temperature (T_c) and phonon dispersion to other known 2D structures like manganese phthalocyanine (MnPc) and CrPP. The authors also note that the predicted 2D VPP is quite suitable for use in flexible spintronic devices. A similar study with Fe, Co, Li, Zn, and H₂PPs was done by Zhu et al. [64] who reported that H₂, Li, and Zn PPs behave as direct bandgap semiconductors while Fe, and Co PP behave as half-metals.

They also report that 2D PP systems behave like n-type semiconducting materials with strong electron mobilities, which were obtained using PDFT combined with Boltzmann transport method with relaxation time approximation. An interesting PDFT study of porphyrin nanosheets and nanowires fused at meso-meso-, β - β -, and β - β -linked array (referred to as SA) and a directly β -fused array (referred to as SB), was performed by Yamaguchi [65]. In this study it was reported that the bandgaps of nanosheets is slightly lower than the nanowires and more importantly it was found that SA type linked arrays have significantly lower bandgaps than SB type. Another example of fused polyporphyrins (PP) with pyrazine linkage was performed by Kumar et al. [66] with transition metals Cr, Mn, Fe, Co, Ni, Cu, and Zn at the porphyrin cores of the nanosheet. Using PDFT calculations with GGA-PBE [45] and GGA+U [67,68] approaches, it was shown that metal PPs have excellent thermal stability with the MnPP system having a ferromagnetic character and half-metallic behavior.

Instead of 2D polyporphyrin (PP) nanosheets, nanowires of 1D PPs were also studied using PDFT. Some 1D porphyrins are also referred to as tape porphyrins in the literature. Gao et. al. [69] studied the electronic structure of metal-polyporphyrin (MPP) and metal-polyhexaphyrin (MPHP) tapes using GGA-PBE functionals. While different MPHP and MPP (M = Co, Ni, Cu, Zn, and Ru) tapes were studied for their conductive (metals/half-metals/semiconductors) behavior, it was reported that doubly linked CoPHP, NiPHP, and double, triple-linked RuPP has half-metallic nature with potential applications for spintronic devices. Zheng et al. studied 1D PP nanowires linked with acetyl linkers with various transition metals (Cr, Mn, Co, Ni, Cu, and Zn) in the porphyrin cores using GGA-PBE [45] and GGA+U [67,68] functionals. Of all the PPs, ZnPP and NiPP nanowires are nonmagnetic while the rest are magnetic with magnetic moments like their corresponding monomer structures. Among all the metal-PP nanowires with acetyl linkers, only MnPP nanowires exhibit half-metallic behavior.

3. PDFT Simulations of Porphyrins on Surfaces

Porphyrins have extended pi-electronic structures which makes them excellent candidates for adsorption on surfaces. They can also bind covalently to substrates through selective meso, α , β , peripheral substituents. PDFT simulations of porphyrins on surfaces are aimed to understand the adsorption configurations, surface reactivity, binding energetics, charge distribution, and transport at surfaces and interfaces and the corresponding magnetic and electronic properties (DOS and band structure) when porphyrin bind to substrates. In this section we present a survey of various PDFT simulations of porphyrins on surfaces based on the type of porphyrin, type of substrate, and application of interest.

3.1. Conformational Studies of Meso-Substituted Porphyrins on Substrates

Meso-substituted porphyrins have multiple structural configurations due to the flexibility of the porphyrin molecule [70]. When porphyrins adsorb on atomically flat conductive surfaces, scanning tunneling microscopy (STM) is used as the preferred technique [71] to understand their surface structures. The adsorption configuration of meso-substituted porphyrins cannot be easily obtained from STM alone due to the limits of STM resolution and structural flexibility of meso-substituted porphyrins. Figure 6 shows some typical confirmations of meso-substituted porphyrins on the surface. Thus, PDFT simulations are complimentary to experimental studies of conformation of porphyrins on substrates. One of the earlier PDFT studies of meso-substituted porphyrins on surfaces was performed by Zotti et al. [72] who studied the adsorption of freebase tetrapyrrolyl porphyrin (TPyP) and FeTPyP on Ag(111). The PDFT simulations were performed with GGA-PW91 [59] functional in conjunction with STM experiments. It was reported that TPyP adsorbs in a flat geometry at 5.6 Å from the surface. The dihedral angle of the pyridyl rings is found to be 70° with adlayer structure primarily directed by lateral intermolecular interactions. Another PDFT study of MnTPyP on Cu(111) [73] with GGA-PBE [45] showed that MnTPyP adsorbs in a saddle shape due to the rotation and inclination of the pyridyl groups towards Cu adatoms, which stabilize the metal-organic chains.

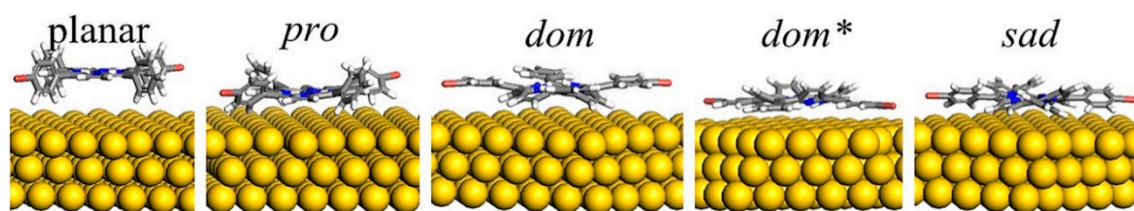


Figure 6. Typical conformations of meso-substituted tetraphenyl porphyrins on a surface. Reprinted with permission from reference [74] Copyright 2017 American Chemical Society.

Metalated and non-metalated meso-substituted phenyl porphyrins are some of the extensively studied porphyrins on surfaces [71]. Like the TPyP porphyrins, tetra-phenyl porphyrins (TPP) have high degree of structural flexibility. Rojas et al. [75] studied the adsorption of freebase TPPs on Ag(111) and Cu(111) metal substrates using GGA-HCTH functional [76,77]. They reported that TPPs form a 2D network on Ag(111), driven by attractive intermolecular interactions, small migration barrier, and minimal charge transfer. In contrast 2H-TPP/Cu(111) has significant charge transfer, resulting in repulsive forces between the molecules that prevent molecular adlayer network formation. A similar result was observed by Lepper et al. [78] who reported an inverted TPP on Cu(111) surface due to coordination of the two iminic nitrogen atoms to the Cu(111) surface via their lone pairs and thus significant charge transfer.

Extensive PDFT studies of adsorption of 3d transition metal (TM) TPP (TM = Co [79–82], Ni [83]) molecule on Ag and Cu substrates were done by various research groups. Both LDA and GGA functionals were used to study the TM-TPP/substrate system. CoTPP on Ag(111) and Cu(111) surfaces exhibited two adsorption properties: first, an asymmetric saddle deformation of CoTPP with an enhanced tilting of the upwards bent pyrroles and second, a single adsorption site where the Co center occupies a bridge position and one molecular axis aligned with the [1-10] substrate direction [79]. On Cu(110) [81], CoTPP molecules adsorb at the short-bridge site with substantial chemical interaction between the molecular core and the surface causing the porphyrin macrocycle to accommodate close to the surface in a flat geometry, which induces considerable tilting distortions in the phenyl groups. NiTPP [83] also has an asymmetric saddle deformation on Cu(111) with observed chemical shifts of Ni $2p_{3/2}$ caused by Ni 3d orbital interaction with Cu(111) substrate.

Due to their structural flexibility, meso-substituted porphyrin molecules interact with surface adatoms on metallic substrates. Hötger et al. [84] studied the surface transmetalation of central metals in TPP and TPyP molecules on Au(111) surface. They reported that Fe^{+2} cation of FeTPP can be replaced by Co in a redox transmetalation-like reaction on Au(111) surface. Likewise, Cu can be replaced by Co. The reverse reaction does not occur, i.e., Fe does not replace Co in the porphyrin. The mechanism and energetics for the surface transmetalation reaction was determined using PDFT calculations with GGA-PBE [45] functional and DFT-D3 [53,85] van der Waals (vdW) corrections. They also report that while identical transmetalation in TPyP molecules were observed, they are not prevalent as in TPP molecules. The reason for this is attributed to peripheral pyridyl groups offering additional coordination sites for the metals, thus suppressing the metal exchange. Moreno-López et al. [86], used PDFT studies with GGA-PBE [45] with DFT-D3 [53,85] and vdW-DF [43,48] functionals to understand the adsorption and coupling of Cl_4 TPP molecules on Cu(111). Using DFT, they reported two coupling reaction pathways: direct dechlorination and Cu adatom-mediated Ullmann coupling. The latter is barrierless, whereas the former faces a barrier of about 0.9 eV for inverted Cl_4 TPP on Cu(111). Adatoms of Au(111) also interact with H_2 TPP [87] forming different surface electronic structures. These observations were confirmed by simulated STM images from PDFT calculations of H_2 TPP on Au(111) in various configurations.

Tetraphenyl porphyrins on non-metallic substrates have also been studied using PDFT simulations. Bassiouk et al. [88], studied the self-assembly of H_2 TPP, CoTPP, and NiTPP molecules on HOPG (highly ordered pyrolytic graphite) surface using STM. It was reported that these TPP molecules only adsorb

at surface defects due to weak pi-pi or vdW interactions between TPPs and HOPG. PDFT calculations were performed to understand the TPP adsorption at the step edges and defects of HOPG. Simulations with PW91 [59] LDA functional showed that the electronic structure is modified significantly at the surface defects and edges of HOPG causing the adsorption and nucleation TPP molecules. TPP molecules on SiC(110) substrate were studied by Catellani et al. [89] using PDFT with GGA-PBE [45]. The sensitization of SiC(110) substrate based on the adsorbed components of a TPP like pyrrole group, phenyl group, and the whole TPP molecule was studied. It was reported that none of these molecules changes the polarity of the SiC(110) substrate even with dispersion interactions. El Garah et al. [90], and Boukari et al. [91], studied the adsorption of Cu-5,10,15,20-tetrakis(3,5-ditert-butyl-phenyl) porphyrin (Cu-TBPP) on Si(111) and boron-defect Si(111)-B surfaces respectively using PDFT simulation and in both cases the CuTBPP confirmations on the substrate were determined.

All the PDFT studies of meso-substituted porphyrins listed above involve aromatic substituents in the meso positions. PDFT studies of meso-substituted porphyrins with tetra-alkyl groups were also reported in the literature. Chin et al. [92] studied the adsorption of tetranonadecyl ($C_{19}H_{39}$) porphyrin on HOPG using STM and DFT. While the structural optimization was carried with molecular DFT, the authors used to determine the STM structure with PDFT simulations with GGA-PW91 [59] functional. Due to long alkyl chains in the molecule, ONIOM [93] method with quantum mechanical simulations on the porphyrin macrocycle and molecular mechanics simulations on alkyl substituents was used to determine the optimized geometries. The STM simulation of the optimized structure matched with STM experiments. In a later study, Reimers et al. [94], studied the adsorption of tera-alkyl porphyrins with alkyl chain lengths (C_nH_{2n+1} with $n = 6-28$) on HOPG using multiple computational methods. It was reported that molecular QM/MM calculations and PDFT calculations with PBE-D3 method predicted similar properties for the chain-length dependence of monolayer formation and polymorphism.

3.2. Conformational Studies of Non-Meso-Substituted Porphyrins on Substrates

Porphyrins without the meso substituents lack the structural flexibility of meso-substituted porphyrins [70]. Octaethylporphyrins (OEP) are some of the commonly studied non-meso-substituted porphyrins on substrates [71] using STM. Fanetti et al. [95] studied the adsorption of CoOEP on Ag(110) surface and reported that CoOEP molecule bind to Ag(110) with a tilt angle of 15° with respect to the substrate due to strong hybridization of the adlayer with the Ag substrate which the authors confirm by PDFT simulations using GGA-PBE [45] functional. Kim et al. studied the adsorption of PtOEP molecule on bare Au(111) and on NaCl/Au(111) surfaces using STM and PDFT with GGA-PBE [45] functional and reported that the top of the valence band has a downward shift in NaCl/Au(111) substrate relative to Au(111). In either of these studies, the adsorption energy of OEP molecules on these substrates has not been reported.

A first comprehensive study of OEP on substrates using PDFT simulations was reported by Chilukuri et al. [96]. It was reported that using standard GGA [45] and LDA [97] functionals would significantly underestimate the adsorption energies of porphyrins on substrates compared to calculations using van der Waals corrected DFT methods like vdW-DF [43,48] or DFT-D3 [53,85]. The binding energies of CoOEP on Au(111) with GGA functional was reported to be -0.31 eV, while the value is -4.34 eV with vdW-DF functional. On HOPG the binding energies are -1.18 and -2.42 eV with LDA and vdW-DF functionals respectively. These results indicate that traditional LDA and GGA functionals significantly underestimate dispersion energies with metallic substrates but to a lesser degree with carbon supports. The authors also report the interfacial charge redistribution, DOS and work function changes upon adsorption of CoOEP on substrates. They also reported the first PDFT simulated bias dependent STM images (Figure 7) of OEP molecules on Au(111) and HOPG which matches with experimental observations. The advantage of using dispersion DFT methods on OEPs is further corroborated by Tada et al. [98], who reported that $Rh^{III}(OEP)(Cl)$ molecule would not have bound to the basal plane of HOPG if not for dispersion corrected DFT functional.

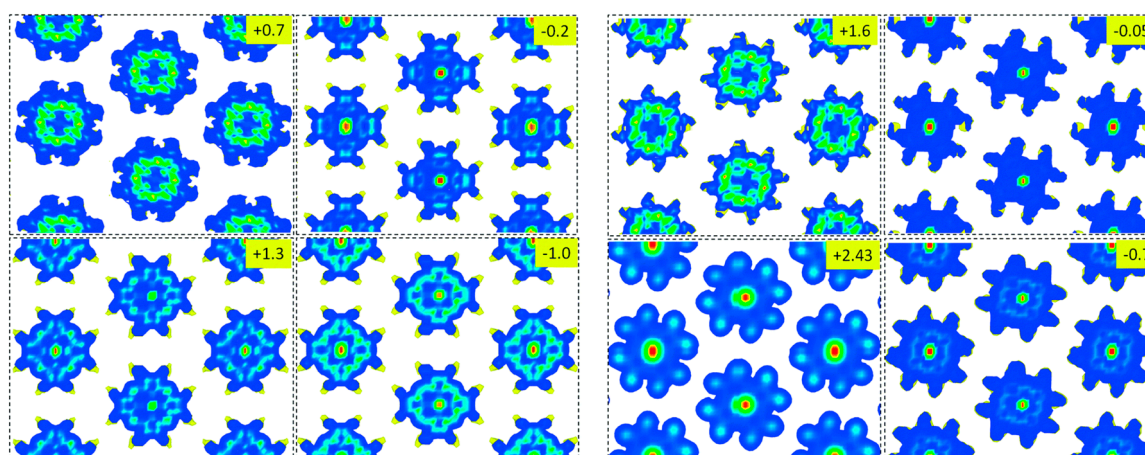


Figure 7. PDFT simulated bias-dependent STM images of Cobalt Octaethylporphyrins (OEP) on Au(111) and HOPG surfaces. Reproduced from reference [96] published by the PCCP Owner Societies.

Iron based haem(b) porphyrin has tetraethyl and tetramethyl substituents in the non-meso positions. Sena et al. [99], studied the adsorption of haem(b) porphyrin on Si(111):H substrate using GGA-PW91 [59] functional and determined the STM images using Tersoff-Hamann approach [100]. The binding energy was estimated to be only 0.42 eV which is likely significantly underestimated because they did not include dispersion interactions in their functional.

Non-substituted porphyrins (P) are also studied extensively using PDFT simulations. Hanke et al. [101], used PDFT simulations with GGA-PW91 [59] and vdW-DF [43,48] functionals to determine the surface configurations of H₂P molecule on Cu(110) surface and the respective adatom interactions were reported. A similar study was performed by Dyer et al. [102], using vdW-DF method who reported that H₂P is chemisorbed to the surface, caused by electron donation into down-shifted and nearly degenerate unoccupied porphine π -orbitals accompanied with electron back-donation from molecular π -orbitals. Miller et al. [103], reported the electronic and spin structure of FeP on Pt(111) surface using multiple vdW-DF [43,48] and functionals with added Hubbard U term. They report that vdW-DF-optPBE and vdW-DF-optB88 functionals found the same binding site to be the most stable and yielded binding energies that were within ~20% of each other, whereas vdW-DF-revPBE functional were substantially weaker. One of the earlier PDFT studies of porphine adsorption was done by Leung et al. [104] using MnP and PdP porphyrins on Au(111). DFT+U [68] technique with PDFT simulations using LDA [97] functionals were used to determine the face-on and side-on interactions of porphyrins on Au(111) substrate. Buimaga-Iarinca et al. studied the effect of translation on binding energy for transition-metal (V, Cr, Mn, Fe, Co, Ni) porphyrins adsorbed on Ag(111) surface using vdW-DF-cx [105]. They concluded that the bridge positions of Ag(111) are favorable for all transition metal porphyrins.

PDFT calculations of not porphyrins but porphyrin-based molecules are also studied in the literature. For example, Zhang et al. studied the adsorption of Ni(Salophen) molecule on Au(111) surface using vdW-DFT functionals and determined the adsorption energy to be 2.74 eV which is about 2/3 of the adsorption energy of similar porphyrin [96,106] molecules on Au(111). Gurdal et al. studied the adsorption of pyrphyrin molecules on Au(111) [107] and Ag(111) [108] surfaces using various GGA and vdW-GGA functionals. They reported the effect of surface herringbone reconstruction of Au(111) surface on the adsorption dynamics of Co(Pyrphyrin) molecules. It was reported that the dominant contribution to the adsorption energy are dispersion forces, followed by the interaction of the cyano groups with the metal. The monolayer formation and geometrical configuration of the assembly are mainly driven by the molecule/molecule interactions.

Surface adsorption of porphyrins as part of a multicomponent mixture were also studied using PDFT simulations. Jahanbekam et al. [109], reported the competitive adsorption of CoOEP and coronene molecules as a function of concentration at the 1-phenyloctane/Au(111) solution solid interface using

STM. In this work, it was reported that CoOEP prefers to bind to the substrate unto a molar ratio of more than 55:1 coronene:CoOEP. At 55:1 ratio, only coronene molecules are seen on the Au(111) surface with STM. Using PDFT simulations of coronene, CoOEP, and coronene:CoOEP models, that authors reported that the strong preference of CoOEP binding to Au(111) is that CoOEP has about ~ 1.8 times larger binding energy than coronene on Au(111). vdW-DF functionals with PAW pseudopotential basis sets were used to determine the adsorption energetics. Additionally, they report that the 1-1 coronene:CoOEP (A in Figure 8) structure is stable between 22:1 to 45:1 molar ratios because the ethyl groups of the CoOEP molecule trap the coronenes on to the Au(111) surface until further changes in the molar ratios. Additionally, the authors used PDFT calculations to determine the interfacial charge distribution (B in Figure 8) and potential energy surfaces for adsorption of CoOEP and coronene molecules on Au(111) surface and used these energies to determine the vibrational frequencies for molecular desorption. It is important to note that coronene molecules exhibit cooperativity and coverage dependency [110] when desorbing from Au(111) substrates.

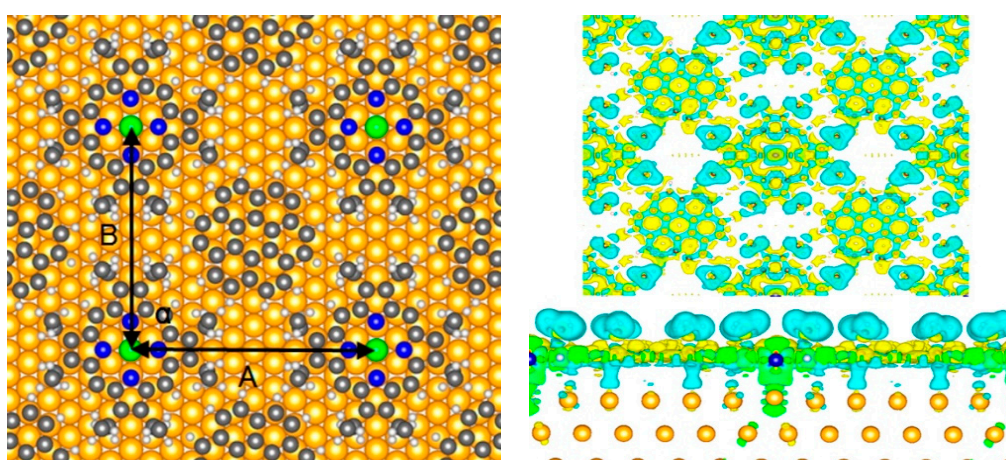


Figure 8. Model of coronene:CoOEP 1:1 structure (A) with corresponding surface charge distribution (B) obtained from PDFT simulations. Reprinted with permission from reference [109] Copyright 2015 American Chemical Society.

3.3. Porphyrins on Single Layer Substrates

Porphyrins can be used for functionalizing and tuning material properties of various single layered substrates like graphene, carbon nanotubes (CNT) and boron nitride (BN) nanotubes. PDFT simulations were used to study the binding and functional changes caused by porphyrins on such substrates. Touzeau et al. [111], studied the adsorption of Metal (Fe, Zn, Mn, Ti) TPP and Zn tetraalkyl porphyrins on graphene surface using PDFT with GGA-PBE [45] functional. The goal was to understand the effect of the peripheral substituents and metal-centers of porphyrins on the functionalization of graphene. PDFT simulations revealed that graphene functionalization with porphyrin-like molecule is suitable for band-gap opening in graphene. They showed porphyrin adsorption on graphene is controlled by the size of the atomic radii, the occupation of the metal 3d orbitals and the host porphyrin structure. Zeng et al. [112], used PDFT simulations to study the spin filter characteristics metal ($M = \text{Cr, Mn, Fe, Co}$) porphyrins functionalized to edges of graphene. Using LDA functional and non-equilibrium Green's functions (NEGF) [113], they determined that Mn-porphyrin bound to graphene exhibits an extremely high spin polarization coefficient in a parallel magnetic configuration which plays a significant role in making a high-performance spin filter.

Functionalization of single walled carbon nanotubes (SWCNT) with various metalloporphyrin ($M = \text{Co, Ni, Cu, Zn}$) molecules using PDFT simulations was reported Zhao et al. [114]. The authors used semiconducting (10,0) and metallic (6,6) SWNTs for functionalization studies using the GGA-PBE [45] functional. DFT calculations indicate that porphyrins can be used to separate

conducting vs. semiconducting in SWCNTs. This is due to hybridization and charge transfer between porphyrins and CNTs. Additionally, metalloporphyrins were found to retain unpaired electrons during functionalization which makes the porphyrin-CNT system a good candidate for optical and spintronic devices. Correa et al. [115], determined the optical response from freebase, Zn-porphyrins/CNT and phthalocyanine/CNT systems using PDFT simulations with vdW-DF [43,48] functionals. They propose that CNT-porphyrins and CNT-phthalocyanines have variable absorption in the visible region, thereby causing increased conversion energy efficiency in an optical device made with both macrocycles. Another interesting study on functionalization of SWCNTs with porphyrins is conducted by Ruiz-Tagle et al. [116], by comparing the effect of physisorption and chemisorption of FeP on metallic and semiconducting SWCNTs. For physisorption studies, LDA [97] functional with vdW-DF [43,48] formalism was used while only LDA [97] functional was used for chemisorption study. The results showed that non-covalent functionalization caused the least change in the electronic and optical properties of SWCNTs. On the other hand, covalent functionalization with metallic SWCNTs would have better electrocatalytic properties than with semiconducting SWCNTs. Porphyrins were also used for functionalizing boron nitride nanotubes (BNNT) similar to SWCNTs. Zhao and Ding [117] performed a PDFT study of BNNT functionalized with metalloporphyrins ($M = \text{Fe, Co, Ni, Cu, Zn}$) using GGA-PBE [45] functional. The authors found that metalloporphyrins energetically prefer to bind the metal with the binding energies ranging from 0.17 to 0.91 eV.

3.4. Porphyrins on Oxide Supports

Porphyrins are widely used as dyes in dye sensitized solar cells where the solar energy trapped by porphyrins is transferred into conductive oxide substrates like TiO_2 , ZnO, etc. In this section, we present a collection of PDFT studies involving interactions of porphyrins with oxide supports used in photovoltaic devices and in catalysis.

Gomez et al. [118], used PDFT simulations with GGA-PW91 [59] functionals to study the surface interactions and charge transfer of [COOH-TPP-Zn(II)] porphyrin on $\text{TiO}_2(110)$ surface. Using PDFT simulations they identified the stable binding site for the anchoring group ($-\text{COO}^-$) to the TiO_2 surface that facilitates electron injection. Using frontier orbitals and DOS from DFT simulations, the authors report that Zn(II) porphyrin is capable of electron injection into TiO_2 , as has been shown from experiments. A similar study was performed by Lin et al. [119], and they used PDFT simulations to study the optical and charge transfer properties of Zn porphyrin adsorbed on the TiO_2 surface. If the $\text{TiO}_2(110)$ surface is hydroxylated, Lovat et al. [120], showed that the iminic nitrogens of free base porphyrins (OEP, TPP, and tetra-butyl TPP) capture the hydrogen atoms from the $\text{TiO}_2(110)$ surface. They used x-ray photoelectron spectroscopy (XPS) experiments combined with PDFT simulations using GGA-PBE [45] functional and DFT-D corrections, and showed the favorable energetics and mechanism for hydrogen capture by porphyrins.

In-situ metalation of TPP using Ni atoms adsorbed on $\text{TiO}_2(110)$ surface was studied by Wang et al. [121] using STM. PDFT simulations were done with the DFT-FIREBALL [122] method. STM images and currents were simulated using Keldysh-Green function formalism. The surface electronic structure from STM experiments matched with the simulated STM images. PDFT simulations [123] are also used to determine the band gap of porphyrin MOFs adsorbed on $\text{TiO}_2(110)$ surface, and it was found that HSE06 functional [47] predicted the bandgap and TiO_2 structure matching the experimental data. Xie et al. [124], studied the effect of asymmetric modification of meso-substituents of TPPs on $\text{TiO}_2(110)$ using PDFT simulations. Experiments have shown that asymmetric modifications can improve the light-harvesting properties and enhance the electron distribution, but the surface adsorbed structure was unknown. In this work, the authors used molecular and PDFT simulations with GGA-PW91 [59] functional to optimize the adsorption geometries of various asymmetric meso-substituted porphyrins on TiO_2 and determine their electronic properties. While TiO_2 is the extensively used oxide support for many PDFT simulations involving porphyrin binding, supports like ZnO [125] and SiO_2 [126] are also studied. In the case of ZnO, the support was used as an alternative for TiO_2 in dye sensitized solar cells

and PDFT calculations were used to understand the charge transfer characteristics. SiO₂-porphyrin [126] studies are used to determine the binding strength for porphyrins to SiO₂ support for application as a trapping agent in petroleum industry.

3.5. PDFT Simulations of Substrate Bound Porphyrin Reactions and Catalysis

Porphyrins on solid substrates can act as active sites for various catalysis reactions. PDFT simulations are typically used to determine the reaction mechanisms of catalytic reactions on surfaces. Quinn et al. [127], used Cu porphyrin to functionalize the graphene surface for methane catalytic reaction. Using PDFT simulations with GGA-PBE [45] functional, it was determined that the porphyrin Cu metal center acts as an active site for the direct oxidation of methane to methanol. The PDFT simulations elucidate the step-by-step reaction mechanism and energetics to understand the catalytic reaction with CuP functionalized graphene at the atomic level. The reaction coordinate (Figure 9) and corresponding geometries of the oxidation reaction was obtained using climbing image nudged elastic band method [128,129] and charge analysis using Bader charges [130].

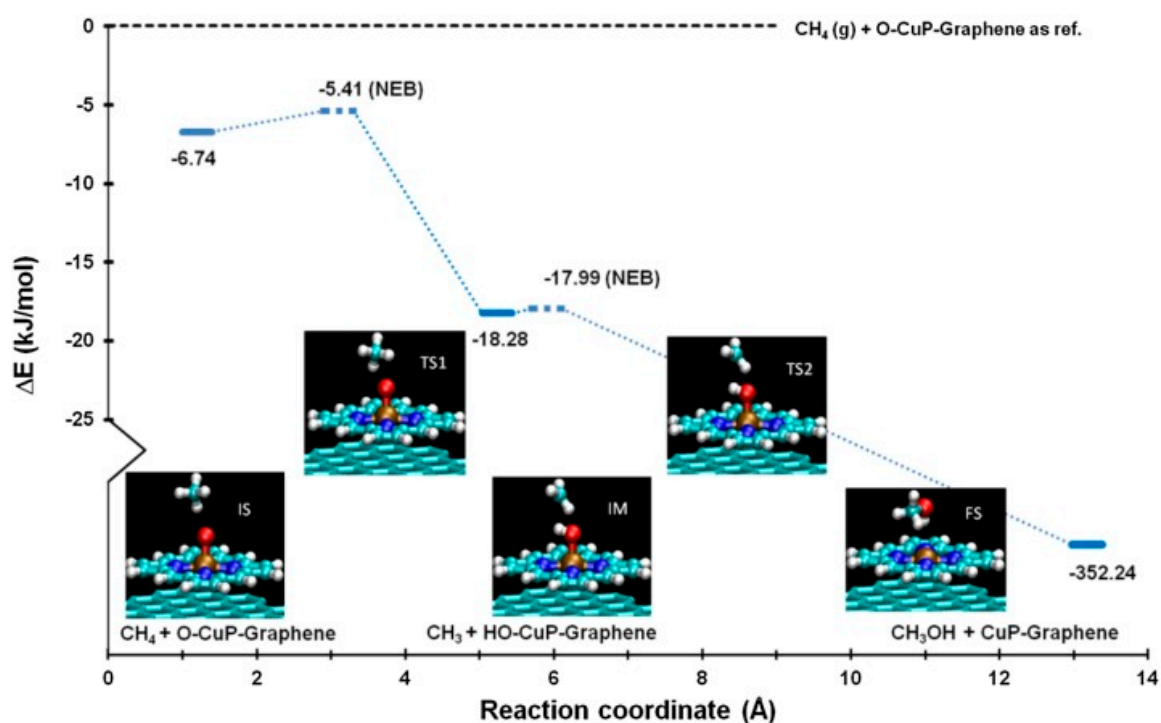


Figure 9. Reaction energy profile for the reaction of CH₄ with pre-adsorbed O atom on CuP functionalized graphene surface. The numbers indicate the energies relative to the reference system of gas phase CH₄ and O bound to the metal center of CuP functionalized graphene surface. The transition states are shown as the maxima on the energy landscape. The x-axis corresponds to the reaction coordinate along the reaction pathway. Reprinted with permission from reference [127] Copyright 2017 Elsevier.

On surface reactions of organic molecules with porphyrins supported on surfaces and monitored by STM experiments has gained significant interest since the pioneering work by Grill et al. [131]. PDFT simulations were used to understand the on-surface reaction mechanisms, energetics and dynamics of porphyrin. Shi et al. [132] studied the Heck reaction of alkene attached aryl bromides to TPP porphyrins on Au(111) surface. The surface structure of TPP changes upon the attachment of the aryl group. The reactions was found to be catalyzed by Pd attached to Au(111) surface. PDFT simulations using GGA-PBE [45] functional with DFT-D3 correction was used to determine the molecular surface configurations during debromination and coupling of Hack reaction on Au(111). Shu et al. [133],

studied the on-surface reactions of aryl-chloride and Cu(111) attached porphyrins. PDFT simulations with GGA-PBE [45] functional and DFT-D3 correction was used to determine the surface reaction dynamics and energetics of dehalogenation, cross coupling and cyclodehydrogenation reactions on Cu(111) surface.

3.6. Magnetic Couplings in Substrate Bound Porphyrins

Porphyrins adsorbed on ferromagnetic substrates can act as excellent candidates for spintronic devices. The ferromagnetic substrates typically involve Co or Ni films deposited on metallic substrates. Mn, Fe, Co, Ni, and Cu porphyrins on Co and Ni substrates were studied to understand the magnetic coupling between metalloporphyrins and metallic surfaces. PDFT simulations are especially helpful to understand the magnetic properties of porphyrin/substrate systems. Wende et al. [134] studied the adsorption of FeOEP on Ni and Co films bound to Cu(100) surface using X-ray absorption spectroscopy (XAS) and X-ray magnetic circular dichroism (XMCD). The experiments were combined with PDFT simulations of corresponding porphyrin/substrate systems using GGA-PW91 [59] functional and DFT+U approach [68]. Binding energetics of ClFeOEP and FeOEP on Co and Ni substrates were determined, and it was noted that the porphyrin loses Cl⁻ upon adsorption. PDFT simulations provided a deeper understanding of Fe-substrate exchange coupling from DOS, charge analysis and magnetization densities. A similar study with free base and Fe porphyrins on Co substrate was carried out by Oppeneer et al. [135] also using GGA-PW91 [59] functional and DFT+U approach [68]. The PDFT simulations were used to understand the origins of the substrate induced magnetic ordering of metalloporphyrins. It was demonstrated that FeOEP ferromagnetically exchange couples, while ClFeOEP antiferromagnetic couples with the substrate. The same research group also studied the magnetic coupling of FeOEP on $c(2 \times 2)$ oxygen reconstructed Co(100) surface [136] with the same PDFT methodology as their earlier studies and showed that FeOEP couples antiferromagnetically with oxygen reconstructed Co(100) surface.

Magnetic coupling with Mn porphyrins on Co substrates was studied by Ali et al. [137] using GGA-PW91 [59] functional and DFT+U approach [68]. The authors reported that Mn porphyrins can adsorb or chemisorb on the Co substrate with MnP-Co binding distances at 3.5 Å and 2.1 Å, respectively. This variable surface binding caused distinct magnetic exchange interactions between porphyrin and substrate, but it was found that Mn magnetic switching occurs at both binding distances. Chylarecka et al. [138] showed that ClMnTPP porphyrin involves in indirect magnetic coupling with Co substrate using PDFT and, STM, XAS, and XMCD studies. GGA-PBE [45] functional with Gaussian type orbitals and with DFT+U approach were used to determine the surface DOS and magnetic properties of ClMnTPP on Co substrate. It was found that if the chloride ion of the MnTPP molecule orients away (Co-Mn-Cl) from the Co surface, a weak ferromagnetic molecule-substrate coupling is observed. PDFT simulations with DFT+U approach were also used to understand the magnetic coupling interactions of Co porphyrins on Ni [139] and graphene [140] substrates.

3.7. Porphyrin Molecular Junctions

Porphyrins and substituted porphyrins were widely studied in single molecule junctions [14]. These junctions typically involve a molecule covalently linking two electrodes. PDFT studies were used to understand the binding and charge transport properties of the molecule and electrodes in the junction. Lamoen et al. [141] performed one of the early studies of the covalently bound Pd porphyrin to gold electrode. They studied the side on (hydrogens of one pyrrole) interactions of Pd porphyrin on Au(111) using the LDA functional. Although this initial model is not a full Pd porphyrin molecular junction (because only one gold electrode was used), the simulation was helpful to gain atomic level understanding of rectifying behavior and charging effects associated with molecular conduction via single-electron tunneling. Another study with the same Pd porphyrin in a one sided junction with Al(111) electrode was performed by Picozzi et al. [142], with both LDA-PW [59] and

GGA-PBE [45] functionals. The energy level alignments, binding energy, and DOS were calculated, and it was reported that PdP/Al(111) interaction is weak yet rectifying.

PDFT study of a complete junction involving a porphyrin sandwiched between two gold electrodes was conducted by Long et al. [143]. A nonequilibrium Green's functions (NEGF) [113] approach with PDFT was used to determine the electron transport properties of the porphyrin molecular junction. The porphyrin molecule is linked to the gold electrodes through two (5,15)-meso-diphenyl substituents. In addition, the role of electron donating and withdrawing substituent (at the 10-meso position) on the electron transport properties was determined. The authors report a negative differential resistance behavior from PDFT calculations which is a critical property for many molecular electronics applications. In another PDFT study, An et al. [144] studied high efficiency switching in porphyrin ethyne benzene/gold molecular junction using GGA-PBE functional. The electron transport properties from PDFT simulations indicated that ethyne-bridged phenyl porphyrin molecules are good candidates for molecular switching devices. The rotation of the phenyl substituent allows for high and low currents due to change in orbital overlaps upon rotation. Additionally, placing amino and nitro substituents caused high ON/OFF current ratios with larger substituent effect when entire porphyrin molecule is in a co-planar geometry than in perpendicular configuration.

Liu et al. [145], developed an optimally-tuned range-separated hybrid (OT-RSH) functional [146] using DFT+ Σ method [147,148] and NEGF [113] approach for accurate description of molecular conduction in junctions. The effect of central metal ($M = 2H, Ni, Co, Cu$) of porphyrins in the molecular conductance between two gold electrodes was studied using PDFT simulations. It was reported that changing the central metal can change the conductance by nearly a factor of 2. Cho et al. [149], studied magnetic and charge transport properties of a metal ($M = H_2, Cr, Mn, Fe, Co$) porphyrin array (PA_∞) connected through thiol groups to two gold electrodes. PDFT simulations with GGA-PBE functional and NEGF formalism was used to determine the conductance and band structure of metal porphyrin junction. It was reported that $CrPA_\infty$ exhibits half-metallic behavior originating from the high spin state of Cr which causes spin asymmetry of the conduction band in $CrPA_\infty$. Additionally, it was reported that spin-filtering ability occurs with an array size of 2, $Cr-PA_2$. Sedghi et al. [150] studied the effect of the length of the substituent side chain in oligo porphyrin molecular wires on the long-range electron tunneling and conductance properties in molecular junction. Three oligo-porphyrins with oligomer length of 1, 2, 3 were sandwiched between gold electrodes and, PDFT simulations and scattering theory were used to study the molecular conductance. It was reported that phase-coherent tunneling occurs through the whole molecular junction.

Graphene and carbon nanotubes (CNT) were also used as electrodes in porphyrin molecular junctions. Suárez et al. [151] studied the low voltage transport response of porphyrin molecular wires bridging two graphene sheets via physisorption. They used the vdW-DF [43,48] functional to study the Breit-Wigner molecular resonances as a function of translation of graphene sheets and porphyrin wires. It was reported that the conductance values are dependent upon the sampling of k-points during simulation. Li et al. used PDFT simulations to study the molecular conductance of porphyrin bridged CNTs. Maximally localized Wannier functions (MLWF) in conjunction with NEGF formalism was used to determine the conductance and quantum interference in the transport properties of porphyrin/CNT junctions. Using molecular conductance data, they reported that tape porphyrins can act as molecular size memory units with many-valued logic.

3.8. Ligand-Porphyrin Reactions on Surfaces

Central metals in metalloporphyrins can react with many axial ligands [152] forming porphyrin-ligand complexes. These ligands can be mono or bi-axial leading to pentavalent and hexavalent complexes. When metalloporphyrins bind to solid surfaces, the surface may act like an axial ligand in the fifth coordination site [153–155]. In this section we present a collection of PDFT studies on coordination of ligands to metalloporphyrins that are adsorbed to surfaces. Coordination of gaseous molecules like CO [156], NO [155], O₂ [157], etc. to porphyrins on surfaces were studied by

various experimental techniques. PDFT simulations were used to understand the binding mechanism of these ligands to substrate bound porphyrins.

Nandi et al. [106], used PDFT simulations with vdW-DF [43,48] functional to understand the binding mechanism of imidazole (Im) ligand to Ni-octaethylporphyrin (NiOEP) bound on HOPG surface. Using STM, solution-spectroscopy, and molecular DFT calculations the authors reported that Im ligand does not bind to NiOEP in solution or in gas-phase but does bind when NiOEP is on the HOPG surface. The reactivity of imidazole toward NiOEP adsorbed on HOPG is attributed to charge donation from the graphite stabilizing the Im-Ni bond (Figure 10). This charge transfer pathway is supported by molecular and periodic modeling calculations which indicate that the Im ligand behaves as a π -acceptor. DFT calculations also show that the nickel ion in the Im-NiOEP/HOPG complex is in a singlet ground state. This is surprising because the gas phase Im-NiOEP complex is found to be stable in a triplet ground state. Integrated charge transfer data (Figure 10) from PDFT also showed that HOPG donates the charge to Imidazole ligand via the NiOEP macrocycle, which indicates that the porphyrin molecule only acts as a charge mediator.

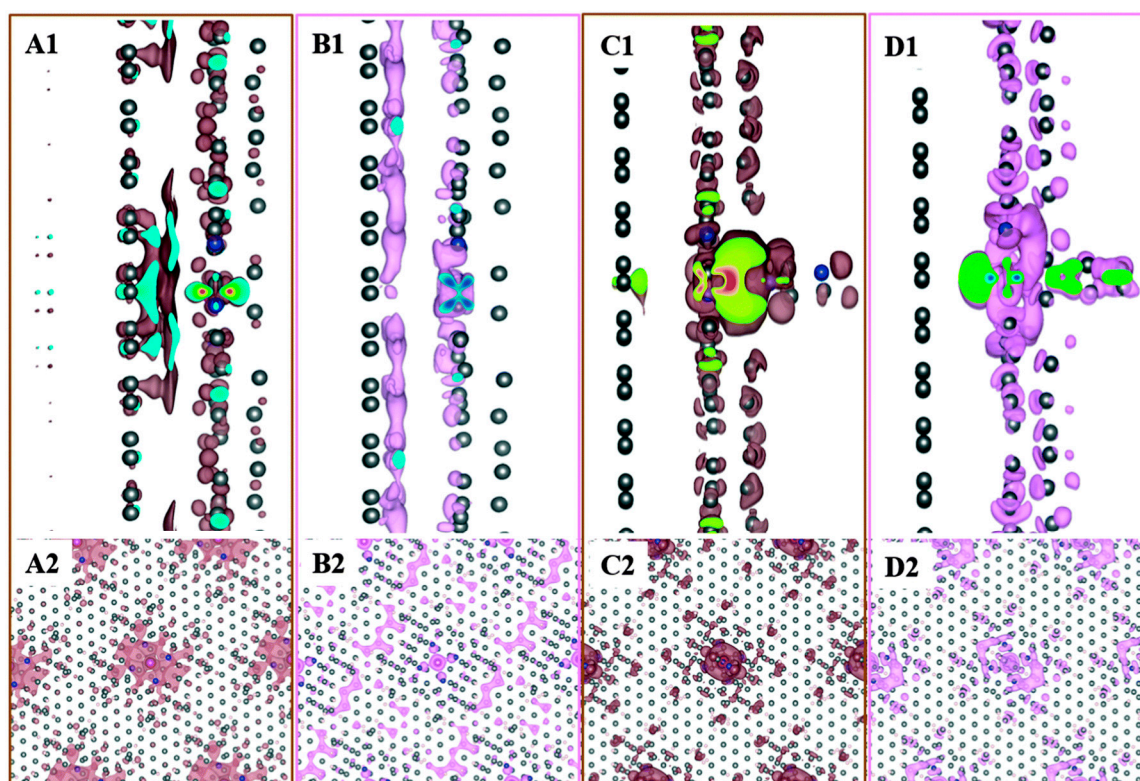


Figure 10. From left to right, charge density difference mappings for positive (colored in brown) and negative (colored in pink) charges for NiOEP/HOPG (A and B) and Im-NiOEP/HOPG (C and D) systems respectively. The images in the top row (A1–D1) represent side-view (along the a-axis) and the bottom row (A2–D2) represent top-view (along c-axis). Element colors are carbon—gray, nitrogen—blue, nickel—yellow (not visible). Hydrogens are masked for clarity. In the cross-section (A1–D1, top row) the rainbow colors (blue to red) indicate charge with blue being highly negative and red being highly positive. Reproduced from reference [106] published by the PCCP Owner Societies.

Binding of gaseous molecules to substrate bound porphyrins using PDFT were carried with tetraphenyl-porphyrins and tape porphyrins. Hieringer et al. [155], reported the ‘surface trans effect’ of NO axial coordination to Co-porphyrin on Ag(111). GGA-PBE [45] functional with dispersion corrections was used to model the NO/CoP/Ag(111) surface and the corresponding structural and energetics were determined. They reported that competition effects, like the trans effect, play a central role and lead to a mutual interference of the two axial ligands, NO and Ag, and their bonds to the

metal center. Wäckerlin et al. [158], used PDFT simulations with DFT+U approach [68] and showed that surface magnetization of porphyrin/ferromagnetic surfaces can be tuned via the choice of axial ligands. NO ($S = 1/2$) and NH_3 ($S = 0$) ligands were used to coordinate with FeTPP and MnTPP porphyrins on Ni and Co ferromagnetic surfaces. PDFT simulations revealed that they reported that the structural trans effect on the surface rules the molecular spin state, as well as the sign and strength of the exchange interaction with the substrate. In another study, Janet et al. [159] compared DFT+U approach and semi-local DFT simulations with GGA-PBE [45] functional using O_2 coordination with CoTPP/Au(111) interface. They reported that semi-local DFT simulations can optimize a structure but DFT+U approach is better for charge and spin predictions in the system. It was also reported that O_2 binding to CoTPP was over stabilized by GGA, while DFT+U predicted reliable energetics especially with spin active systems. Ghosh et al. [160], used DFT+U approach to determine the spin states of CO, NO and O_2 bound to Mn porphyrin on Au(111). The PDFT simulations were used to demonstrate reversible spin-switching of ligand bound porphyrin/Au(111) system by conformations changing of porphyrin structure on the substrate. Ligand binding on porphyrin nanowires were also studied using PDFT simulations. Binding of NO molecule to metal tape-porphyrins [161–163] with PDFT calculations reveal molecular structure of metal tape-porphyrins has negligible change upon ligand binding but considerable change in the electronic structure was observed. Additionally, a significant band gap reduction has been observed upon NO ligand binding.

4. Summary

Periodic density functional theory (PDFT) calculations have been indispensable to bridge the gaps between observable properties at the condensed phase and the electronic structure of the periodic system. They led to fundamental understanding and tuning of the solid-state behavior of many functional materials and interfaces. In this review, a collection of PDFT simulations of porphyrins in nanostructures and on surfaces were presented. Porphyrins are important compounds used for many have numerous biological and technological applications. While many reviews of porphyrins and their derivatives are available in the literature, a review of periodic porphyrin structures has never been reported to our knowledge. We organized the review based on applications of PDFT simulations to understand specific structural, conformational, adsorption, electronic, magnetic, charge transfer properties, and reactivity of porphyrins on surfaces. The typical properties calculated using PDFT simulations include optimized geometries, binding energetics, density of states, band structure, spin switching and magnetization, charge transport, STM images (local electronic structure), reaction intermediates in catalytic reactions, etc. Hence, this review should be of great interest for the porphyrin research community and to the broader audience performing PDFT simulations.

In our survey of periodic simulations on porphyrins with DFT, plane wave pseudopotential basis sets were the predominant choice rather than Gaussian type orbital basis sets. Most of the early simulations were performed with the bottom two rungs of the “Jacob’s ladder” which are the GGA and LDA type functionals. The drawbacks of using these functionals include underestimation of electronic bandgaps and weak dispersion interactions, especially with systems involving organic molecules like porphyrins. LDA overestimates, while GGA underestimates the binding energies in condensed phase systems like transition metal, metal oxides, carbon, and silicon crystals. Both functionals underestimate interactions involving organic molecules like porphyrins.

Recently many PDFT studies were performed with dispersion corrected DFT functionals or with empirical dispersion corrections. Inclusion of vdW interactions greatly improved the calculated binding energies of porphyrins leading to data that better matched experiments. It was reported that dispersion interactions are more important for porphyrins on metallic substrates than on non-metal substrates. Within the last decade hybrid functionals like B3LYP and HSE were used for PDFT simulations of porphyrins. These functionals improved the band gap and geometric optimizations of porphyrin nanostructures and interfaces. Our review of the literature also found that DFT+U is the method of choice for calculations involving magnetically coupled and spin active porphyrin systems. With the

improvement of DFT functionals and computing capability more and more expensive calculations were being performed for a fundamental understanding of porphyrin behavior in periodic systems.

Like many quantum mechanical calculations, PDFT calculations have limitations with respect to the size of the modeled system and accuracy of the energies obtained from DFT calculations. Additionally, choosing the right DFT functional for modeling a heterogeneous periodic system like porphyrins is challenging and no single PDFT functional is deemed appropriate for all applications. Based on the problem of interest like electronic structure, binding energies, excited state properties, etc., a variety of PDFT functionals were used to study bulkier systems like porphyrins and phthalocyanines. Unlike molecular DFT functionals used for porphyrin based systems [24], the number of PDFT functionals are limited especially for performing time-dependent or excited state systems. In addition, simulations of larger periodic systems [110] with PDFT is computationally expensive, while ab initio molecular dynamics (MD) simulations of larger systems are practically impossible.

Funding: This material is based upon work supported by the National Science Foundation under Grant No. (CHE-1800070).

Conflicts of Interest: The authors declare no conflict of interest.

References

1. Huang, H.; Song, W.; Rieffel, J.; Lovell, J.F. Emerging applications of porphyrins in photomedicine. *Front. Phys.* **2015**, *3*, 3. [[CrossRef](#)] [[PubMed](#)]
2. Imran, M.; Ramzan, M.; Qureshi, A.K.; Khan, M.A.; Tariq, M. Emerging Applications of Porphyrins and Metalloporphyrins in Biomedicine and Diagnostic Magnetic Resonance Imaging. *Biosensors* **2018**, *8*, 95. [[CrossRef](#)] [[PubMed](#)]
3. Li, W.; Aida, T. Dendrimer Porphyrins and Phthalocyanines. *Chem. Rev.* **2009**, *109*, 6047–6076. [[CrossRef](#)] [[PubMed](#)]
4. Aziz, A.; Ruiz-Salvador, A.; Hernández, N.C.; Calero, S.; Hamad, S.; Grau-Crespo, R. Porphyrin-based metal-organic frameworks for solar fuel synthesis photocatalysis: Band gap tuning via iron substitutions. *J. Mater. Chem. A* **2017**, *5*, 11894–11904. [[CrossRef](#)]
5. Maldotti, A.; Amadelli, R.; Bartocci, C.; Carassiti, V.; Polo, E.; Varani, G. Photochemistry of Iron-porphyrin complexes. Biomimetics and catalysis. *Coord. Chem. Rev.* **1993**, *125*, 143–154. [[CrossRef](#)]
6. Barona-Castaño, J.C.; Carmona-Vargas, C.C.; Brocksom, T.J.; de Oliveira, K.T. Porphyrins as Catalysts in Scalable Organic Reactions. *Molecules* **2016**, *21*, 310. [[CrossRef](#)]
7. Li, L.; Diao, E.W. Porphyrin-sensitized solar cells. *Chem. Soc. Rev.* **2012**, *42*, 291–304. [[CrossRef](#)]
8. Paolesse, R.; Nardis, S.; Monti, D.; Stefanelli, M.; Di Natale, C. Porphyrinoids for Chemical Sensor Applications. *Chem. Rev.* **2017**, *117*, 2517–2583. [[CrossRef](#)]
9. Jurow, M.; Schuckman, A.E.; Batteas, J.D.; Drain, C.M. Porphyrins as Molecular Electronic Components of Functional Devices. *Coord. Chem. Rev.* **2010**, *254*, 2297–2310. [[CrossRef](#)]
10. Lopes, D.M.; Araújo-Chaves, J.C.; Menezes, L.R.; Nantes-Cardoso, I.L. Technological Applications of Porphyrins and Related Compounds: Spintronics and Micro-/Nanomotors. *Solid State Phys.* **2019**. [[CrossRef](#)]
11. Hoang, M.H.; Choi, D.H.; Lee, S.J. Organic field-effect transistors based on semiconducting porphyrin single crystals. *Synth. Met.* **2012**, *162*, 419–425. [[CrossRef](#)]
12. Hoang, M.H.; Ngo, T.T.; Nguyen, D.N. Effect of molecular packing of zinc(II) porphyrins on the performance of field-effect transistors. *Adv. Nat. Sci. Nanosci. Nanotechnol.* **2014**, *5*, 045012. [[CrossRef](#)]
13. Che, C.; Xiang, H.; Chui, S.S.; Xu, Z.; Roy, V.A.L.; Yan, J.J.; Fu, W.; Lai, P.T.; Williams, I.D. A High-Performance Organic Field-Effect Transistor Based on Platinum(II) Porphyrin: Peripheral Substituents on Porphyrin Ligand Significantly Affect Film Structure and Charge Mobility. *Chem. Asian J.* **2008**, *3*, 1092–1103. [[CrossRef](#)] [[PubMed](#)]
14. Seol, M.; Choi, S.; Kim, C.; Moon, D.; Choi, Y. Porphyrin–Silicon Hybrid Field-Effect Transistor with Individually Addressable Top-gate Structure. *ACS Nano* **2012**, *6*, 183–189. [[CrossRef](#)] [[PubMed](#)]
15. El Abbassi, M.; Zwick, P.; Rates, A.; Stefani, D.; Prescimone, A.; Mayor, M.; Van Der Zant, H.S.J.; Dulić, D. Unravelling the conductance path through single-porphyrin junctions. *Chem. Sci.* **2019**, *10*, 8299–8305. [[CrossRef](#)] [[PubMed](#)]

16. Feixas, F.; Solà, M.; Swart, M. Chemical bonding and aromaticity in metalloporphyrins. *Can. J. Chem.* **2009**, *87*, 1063–1073. [[CrossRef](#)]
17. Senge, M.O.; Fazekas, M.; Notaras, E.G.A.; Blau, W.J.; Zawadzka, M.; Locos, O.B.; Ni Mhuircheartaigh, E.M. Nonlinear Optical Properties of Porphyrins. *Adv. Mater.* **2007**, *19*, 2737–2774. [[CrossRef](#)]
18. Tran-Thi, T. Assemblies of phthalocyanines with porphyrins and porphyrazines: Ground and excited state optical properties. *Coord. Chem. Rev.* **1997**, *160*, 53–91. [[CrossRef](#)]
19. Saito, S.; Osuka, A. Expanded Porphyrins: Intriguing Structures, Electronic Properties, and Reactivities. *Angew. Chem. Int. Ed.* **2011**, *50*, 4342–4373. [[CrossRef](#)]
20. Adinehnia, M.; Eskelsen, J.R.; Hipps, K.W.; Mazur, U. Mechanical behavior of crystalline ionic porphyrins. *J. Porphyr. Phthalocyanines* **2019**, *23*, 154–165. [[CrossRef](#)]
21. Phillips, J.N. Chapter II—Physico-chemical Properties of Porphyrins. In *Comprehensive Biochemistry*; Florin, M., Stotz, E.H., Eds.; Elsevier: Amsterdam, The Netherlands, 1963; Volume 9, pp. 34–72.
22. Jensen, K.P.; Ryde, U. Comparison of the Chemical Properties of Iron and Cobalt Porphyrins and Corrins. *ChemBioChem* **2003**, *4*, 413–424. [[CrossRef](#)] [[PubMed](#)]
23. Brothers, P.J.; Collman, J.P. The organometallic chemistry of transition-metal porphyrin complexes. *Acc. Chem. Res.* **1986**, *19*, 209–215. [[CrossRef](#)]
24. Shubina, T.E. Computational Studies on Properties, Formation, and Complexation of M(II)-Porphyrins. In *Advances in Inorganic Chemistry*; van Eldik, R., Harvey, J., Eds.; Academic Press: New York, NY, USA, 2010; Volume 62, pp. 261–299.
25. Baerends, E.; Ricciardi, G.; Rosa, A.; Van Gisbergen, S. A DFT/TDDFT interpretation of the ground and excited states of porphyrin and porphyrazine complexes. *Coord. Chem. Rev.* **2002**, *230*, 5–27. [[CrossRef](#)]
26. Kepenekian, M.; Calborean, A.; Vetere, V.; Le Guennic, B.; Robert, V.; Maldivi, P. Toward Reliable DFT Investigations of Mn-Porphyrins through CASPT2/DFT Comparison. *J. Chem. Theory Comput.* **2011**, *7*, 3532–3539. [[CrossRef](#)] [[PubMed](#)]
27. Aydin, M. Geometric and Electronic Properties of Porphyrin and its Derivatives. In *Applications of Molecular Spectroscopy to Current Research in the Chemical and Biological Sciences*; IntechOpen: Rijeka, Croatia, 2016; p. 10.
28. Rappoport, D.; Crawford, N.R.M.; Furche, F.; Burke, K. Which functional should I choose? In *Computational Inorganic and Bioinorganic Chemistry*; Solomon, E.I., Scott, R.A., King, B.R., Eds.; Wiley John & Sons, Inc.: Hoboken, NJ, USA, 2009.
29. Liao, M.-S.; Lu, Y.; Scheiner, S. Performance assessment of density-functional methods for study of charge-transfer complexes. *J. Comput. Chem.* **2003**, *24*, 623–631. [[CrossRef](#)] [[PubMed](#)]
30. De Visser, S.P.; Stillman, M.J. Challenging Density Functional Theory Calculations with Hemes and Porphyrins. *Int. J. Mol. Sci.* **2016**, *17*, 519. [[CrossRef](#)]
31. Kratzer, P.; Neugebauer, J. The Basics of Electronic Structure Theory for Periodic Systems. *Front. Chem.* **2019**, *7*, 106. [[CrossRef](#)]
32. Tosoni, S.; Tuma, C.; Sauer, J.; Civalleri, B.; Ugliengo, P. A comparison between plane wave and Gaussian-type orbital basis sets for hydrogen bonded systems: Formic acid as a test case. *J. Chem. Phys.* **2007**, *127*, 154102. [[CrossRef](#)]
33. Kresse, G.; Hafner, J. Ab initio molecular dynamics for liquid metals. *Phys. Rev. B* **1993**, *47*, 558–561. [[CrossRef](#)]
34. Kresse, G.; Furthmüller, J. Efficiency of ab-initio total energy calculations for metals and semiconductors using a plane-wave basis set. *Comput. Mater. Sci.* **1996**, *6*, 15–50. [[CrossRef](#)]
35. Kresse, G.; Joubert, D. From ultrasoft pseudopotentials to the projector augmented-wave method. *Phys. Rev. B* **1999**, *59*, 1758–1775. [[CrossRef](#)]
36. Giannozzi, P.; Baroni, S.; Bonini, N.; Calandra, M.; Car, R.; Cavazzoni, C.; Ceresoli, D.; Chiarotti, G.L.; Cococcioni, M.; Dabo, I.; et al. QUANTUM ESPRESSO: A modular and open-source software project for quantum simulations of materials. *J. Physics: Condens. Matter* **2009**, *21*, 395502. [[CrossRef](#)] [[PubMed](#)]
37. Hutter, J.; Iannuzzi, M.; Schiffmann, F.; Vande Vondele, J. cp2k: Atomistic simulations of condensed matter systems. *Wires Comput. Mol. Sci.* **2014**, *4*, 15–25. [[CrossRef](#)]
38. Clark, S.J.; Segall, M.D.; Pickard, C.J.; Hasnip, P.J.; Probert, M.I.; Keith, R.; Payne, M.C. First principles methods using CASTEP. *Z. Für Krist. Cryst. Mater.* **2009**, *220*, 567. [[CrossRef](#)]

39. Delley, B. DMol, a standard tool for density functional calculations: Review and advances. In *Theoretical and Computational Chemistry*; Seminario, J.M., Politzer, P., Eds.; Elsevier: Amsterdam, The Netherlands, 1995; Volume 2, pp. 221–254.
40. Soler, J.M.; Artacho, E.; Gale, J.D.; Garcia, A.; Junquera, J.; Ordejón, P.; Sánchez-Portal, D. The SIESTA method for ab initio order- N materials simulation. *J. Phys. Condens. Matter* **2002**, *14*, 2745–2779. [[CrossRef](#)]
41. Hutter, J.; Marcella, I. CPMD: Car-Parrinello molecular dynamics. *Z. Für Krist. Cryst. Mater.* **2009**, *220*, 549. [[CrossRef](#)]
42. Adinehnia, M.; Borders, B.; Ruf, M.; Chilukuri, B.; Hipps, K.W.; Mazur, U. Comprehensive structure–function correlation of photoactive ionic π -conjugated supermolecular assemblies: An experimental and computational study. *J. Mater. Chem. C* **2016**, *4*, 10223–10239. [[CrossRef](#)]
43. Klimes, J.; Bowler, D.R.; Michaelides, A. Chemical accuracy for the van der Waals density functional. *J. Phys. Condens. Matter* **2009**, *22*, 022201. [[CrossRef](#)]
44. Blöchl, P.E. Projector augmented-wave method. *Phys. Rev. B* **1994**, *50*, 17953. [[CrossRef](#)]
45. Perdew, J.P.; Burke, K.; Ernzerhof, M. Generalized Gradient Approximation Made Simple. *Phys. Rev. Lett.* **1996**, *77*, 3865–3868. [[CrossRef](#)]
46. Heyd, J.; Scuseria, G.E.; Ernzerhof, M. Hybrid functionals based on a screened Coulomb potential. *J. Chem. Phys.* **2003**, *118*, 8207. [[CrossRef](#)]
47. Brothers, E.N.; Izmaylov, A.F.; Normand, J.O.; Barone, V.; Scuseria, G.E. Accurate solid-state band gaps via screened hybrid electronic structure calculations. *J. Chem. Phys.* **2008**, *129*, 11102. [[CrossRef](#)] [[PubMed](#)]
48. Klimes, J.; Bowler, D.R.; Michaelides, A. Van der Waals density functionals applied to solids. *Phys. Rev. B* **2011**, *83*. [[CrossRef](#)]
49. Borders, B.; Adinehnia, M.; Chilukuri, B.; Ruf, M.; Hipps, K.W.; Mazur, U. Tuning the optoelectronic characteristics of ionic organic crystalline assemblies. *J. Mater. Chem. C* **2018**, *6*, 4041–4056. [[CrossRef](#)]
50. Tian, X.; Lin, C.; Zhong, Z.; Li, X.; Xu, X.; Liu, J.; Kang, L.; Chai, G.; Yao, J. Effect of Axial Coordination of Iron Porphyrin on Their Nanostructures and Photocatalytic Performance. *Cryst. Growth Des.* **2019**, *19*, 3279–3287. [[CrossRef](#)]
51. Krasnov, P.O.; Kuzubov, A.A.; Kholobina, A.S.; Kovaleva, E.; Kuzubova, M.V. Optical charge transfer transitions in supramolecular fullerene and porphyrin compounds. *J. Struct. Chem.* **2016**, *57*, 642–648. [[CrossRef](#)]
52. Boyd, P.D.W.; Hodgson, M.C.; Rickard, C.E.F.; Oliver, A.G.; Chaker, L.; Brothers, P.J.; Bolskar, R.D.; Tham, F.S.; Reed, C.A. Selective Supramolecular Porphyrin/Fullerene Interactions. *J. Am. Chem. Soc.* **1999**, *121*, 10487–10495. [[CrossRef](#)]
53. Grimme, S. Semiempirical GGA-type density functional constructed with a long-range dispersion correction. *J. Comput. Chem.* **2006**, *27*, 1787–1799. [[CrossRef](#)]
54. Gajdoš, M.; Hümmer, K.; Kresse, G.; Furthmüller, J.; Bechstedt, F. Linear optical properties in the projector-augmented wave methodology. *Phys. Rev. B* **2006**, *73*, 045112. [[CrossRef](#)]
55. Hamad, S.; Hernandez, N.C.; Aziz, A.; Ruiz-Salvador, A.; Calero, S.; Grau-Crespo, R. Electronic structure of porphyrin-based metal-organic frameworks and their suitability for solar fuel production photocatalysis. *J. Mater. Chem. A* **2015**, *3*, 23458–23465. [[CrossRef](#)]
56. Fateeva, A.; Chater, P.A.; Ireland, C.P.; Tahir, A.A.; Khimyak, Y.Z.; Wiper, P.V.; Darwent, J.R.; Rosseinsky, M.J. A Water-Stable Porphyrin-Based Metal-Organic Framework Active for Visible-Light Photocatalysis. *Angew. Chem. Int. Ed.* **2012**, *51*, 7440–7444. [[CrossRef](#)] [[PubMed](#)]
57. Liu, J.; Zhou, W.; Liu, J.; Howard, I.; Kilibarda, G.; Schlabach, S.; Couprie, D.; Addicoat, M.; Yoneda, S.; Tsutsui, Y.; et al. Photoinduced Charge-Carrier Generation in Epitaxial MOF Thin Films: High Efficiency as a Result of an Indirect Electronic Band Gap? *Angew. Chem. Int. Ed.* **2015**, *54*, 7441–7445. [[CrossRef](#)] [[PubMed](#)]
58. Liu, J.; Zhou, W.; Liu, J.; Fujimori, Y.; Higashino, T.; Imahori, H.; Jiang, X.; Zhao, J.; Sakurai, T.; Hattori, Y.; et al. A new class of epitaxial porphyrin metal-organic framework thin films with extremely high photocarrier generation efficiency: Promising materials for all-solid-state solar cells. *J. Mater. Chem. A* **2016**, *4*, 12739–12747. [[CrossRef](#)]
59. Perdew, J.P.; Wang, Y. Accurate and simple analytic representation of the electron-gas correlation energy. *Phys. Rev. B* **1992**, *45*, 13244–13249. [[CrossRef](#)] [[PubMed](#)]
60. Perdew, J.P.; Zunger, A. Self-interaction correction to density-functional approximations for many-electron systems. *Phys. Rev. B* **1981**, *23*, 5048–5079. [[CrossRef](#)]

61. Posligua, V.; Aziz, A.; Haver, R.; Peeks, M.D.; Anderson, H.L.; Grau-Crespo, R. Band Structures of Periodic Porphyrin Nanostructures. *J. Phys. Chem. C* **2018**, *122*, 23790–23798. [[CrossRef](#)]
62. Allec, S.I.; Ilawe, N.V.; Wong, B.M. Unusual Bandgap Oscillations in Template-Directed π -Conjugated Porphyrin Nanotubes. *J. Phys. Chem. Lett.* **2016**, *7*, 2362–2367. [[CrossRef](#)]
63. Singh, H.K.; Kumar, P.; Waghmare, U.V. Theoretical Prediction of a Stable 2D Crystal of Vanadium Porphyrin: A Half-Metallic Ferromagnet. *J. Phys. Chem. C* **2015**, *119*, 25657–25662. [[CrossRef](#)]
64. Zhu, B.; Zhang, X.; Zeng, B.; Li, M.; Long, M. First-principles predictions on charge mobility and half-metallicity in two dimensional metal coordination polyporphyrin sheets. *Org. Electron.* **2017**, *49*, 45. [[CrossRef](#)]
65. Yamaguchi, Y. Theoretical study of two-dimensionally fused zinc porphyrins: DFT calculations. *Int. J. Quantum Chem.* **2009**, *109*, 1584–1597. [[CrossRef](#)]
66. Kumar, S.; Choudhuri, I.; Pathak, B. An atomically thin ferromagnetic half-metallic pyrazine-fused Mn-porphyrin sheet: A slow spin relaxation system. *J. Mater. Chem. C* **2016**, *4*, 9069–9077. [[CrossRef](#)]
67. Dudarev, S.L.; Botton, G.A.; Savrasov, S.Y.; Humphreys, C.J.; Sutton, A.P. Electron-energy-loss spectra and the structural stability of nickel oxide: An LSDA+U study. *Phys. Rev. B* **1998**, *57*, 1505–1509. [[CrossRef](#)]
68. Anisimov, V.I.; Aryasetiawan, F.; Lichtenstein, A.I. First-principles calculations of the electronic structure and spectra of strongly correlated systems: Dynamical mean-field theory. *J. Phys. Condens. Matter* **1997**, *9*, 767–808. [[CrossRef](#)]
69. Gao, G.; Kang, H.S. Engineering of the electronic structures of metal-porphyrin tapes and metal-hexaphyrin tapes: A first-principles study. *Chem. Phys.* **2010**, *369*, 66. [[CrossRef](#)]
70. Medforth, C.J.; Senge, M.O.; Smith, K.M.; Sparks, L.D.; Shelnut, J.A. Nonplanar distortion modes for highly substituted porphyrins. *J. Am. Chem. Soc.* **1992**, *114*, 9859–9869. [[CrossRef](#)]
71. Otsuki, J. STM studies on porphyrins. *Coord. Chem. Rev.* **2010**, *254*, 2311–2341. [[CrossRef](#)]
72. Zotti, L.A.; Teobaldi, G.; Hofer, W.A.; Auwärter, W.; Weber-Bargioni, A.; Barth, J.V. Ab-initio calculations and STM observations on tetrapyrrolyl and Fe(II)-tetrapyrrolyl-porphyrin molecules on Ag (1 1 1). *Surf. Sci.* **2007**, *601*, 2409–2414. [[CrossRef](#)]
73. Chen, X.; Lei, S.; Lotze, C.; Czekelius, C.; Paulus, B.; Franke, K.J. Conformational adaptation and manipulation of manganese tetra(4-pyridyl)porphyrin molecules on Cu(111). *J. Chem. Phys.* **2017**, *146*, 092316. [[CrossRef](#)]
74. Zhang, Q.; Zheng, X.; Kuang, G.; Wang, W.; Zhu, L.; Pang, R.; Shi, X.; Shang, X.; Huang, X.; Liu, P.N.; et al. Single-Molecule Investigations of Conformation Adaptation of Porphyrins on Surfaces. *J. Phys. Chem. Lett.* **2017**, *8*, 1241–1247. [[CrossRef](#)]
75. Rojas, G.; Chen, X.; Bravo, C.; Kim, J.-H.; Kim, J.-S.; Xiao, J.; Dowben, P.A.; Gao, Y.; Zeng, X.C.; Choe, W.; et al. Self-Assembly and Properties of Nonmetalated Tetraphenyl-Porphyrin on Metal Substrates. *J. Phys. Chem. C* **2010**, *114*, 9408–9415. [[CrossRef](#)]
76. Hamprecht, F.A.; Cohen, A.J.; Tozer, D.J.; Handy, N.C. Development and assessment of new exchange-correlation functionals. *J. Chem. Phys.* **1998**, *109*, 6264–6271. [[CrossRef](#)]
77. Boese, A.D.; Doltsinis, N.L.; Handy, N.C.; Sprick, M. New generalized gradient approximation functionals. *J. Chem. Phys.* **2000**, *112*, 1670–1678. [[CrossRef](#)]
78. Lepper, M.; Köbl, J.; Schmitt, T.; Gurrath, M.; Siervo, A.d.; Schneider, M.A.; Steinrück, H.; Meyer, B.; Marbach, H.; Hieringer, W. “Inverted” porphyrins: A distorted adsorption geometry of free-base porphyrins on Cu (111). *Chem. Commun.* **2017**, *53*, 8207–8210. [[CrossRef](#)] [[PubMed](#)]
79. Houwaart, T.; Le Bahers, T.; Sautet, P.; Auwärter, W.; Seufert, K.; Barth, J.V.; Bocquet, M. Scrutinizing individual CoTPP molecule adsorbed on coinage metal surfaces from the interplay of STM experiment and theory. *Surf. Sci.* **2015**, *635*, 108–114. [[CrossRef](#)]
80. Weber-Bargioni, A.; Auwärter, W.; Klappenberger, F.; Reichert, J.; Lefrançois, S.; Strunskus, T.; Wöll, C.; Schiffrin, A.; Pennec, Y.; Barth, J.V. Visualizing the Frontier Orbitals of a Conformationally Adapted Metalloporphyrin. *ChemPhysChem* **2008**, *9*, 89–94. [[CrossRef](#)]
81. Donovan, P.; Robin, A.; Dyer, M.S.; Persson, M.; Raval, R. Unexpected Deformations Induced by Surface Interaction and Chiral Self-Assembly of CoII-Tetraphenylporphyrin (Co-TPP) Adsorbed on Cu (110): A Combined STM and Periodic DFT Study. *Chem. A Eur. J.* **2010**, *16*, 11641–11652. [[CrossRef](#)]
82. Auwärter, W.; Seufert, K.; Klappenberger, F.; Reichert, J.; Weber-Bargioni, A.; Verdini, A.; Cvetko, D.; Dell’Angela, M.; Floreano, L.; Cossaro, A.; et al. Site-specific electronic and geometric interface structure of Co-tetraphenyl-porphyrin layers on Ag(111). *Phys. Rev. B* **2010**, *81*, 245403. [[CrossRef](#)]

83. Fatayer, S.; Veiga, R.G.A.; Prieto, M.J.; Perim, E.; Landers, R.; Miwa, R.H.; De Siervo, A. Self-assembly of NiTPP on Cu(111): A transition from disordered 1D wires to 2D chiral domains. *Phys. Chem. Chem. Phys.* **2015**, *17*, 18344–18352. [[CrossRef](#)]
84. Hötger, D.; Abufager, P.F.; Morchutt, C.; Alexa, P.; Grumelli, D.E.; Dreiser, J.; Stepanow, S.; Gambardella, P.; Busnengo, H.F.; Etzkorn, M.; et al. On-surface transmetalation of metalloporphyrins. *Nanoscale* **2018**, *10*, 21116–21122. [[CrossRef](#)]
85. Grimme, S.; Antony, J.; Ehrlich, S.; Krieg, H. A consistent and accurate ab initio parametrization of density functional dispersion correction (DFT-D) for the 94 elements H-Pu. *J. Chem. Phys.* **2010**, *132*, 154104. [[CrossRef](#)]
86. Moreno-López, J.C.; Mowbray, D.J.; Paz, A.P.; Ferreira, R.C.D.C.; Dos Santos, A.C.; Ayala, P.; De Siervo, A. Roles of Precursor Conformation and Adatoms in Ullmann Coupling: An Inverted Porphyrin on Cu(111). *Chem. Mater.* **2019**, *31*, 3009–3017. [[CrossRef](#)]
87. Mielke, J.; Hanke, F.; Peters, M.V.; Hecht, S.; Persson, M.; Grill, L. Adatoms underneath Single Porphyrin Molecules on Au(111). *J. Am. Chem. Soc.* **2015**, *137*, 1844–1849. [[CrossRef](#)] [[PubMed](#)]
88. Bassiouk, M.; Alvarez-Zauco, E.; Basiuk, V.A. Theoretical analysis of the effect of surface defects on porphyrin adsorption and self-assembly on graphite. *J. Comput. Nanosci.* **2012**, *9*, 532–540. [[CrossRef](#)]
89. Catellani, A.; Calzolari, A. Functionalization of SiC(110) Surfaces via Porphyrin Adsorption: Ab Initio Results. *J. Phys. Chem. C* **2012**, *116*, 886–892. [[CrossRef](#)]
90. El Garah, M.; Makoudi, Y.; Palmino, F.; Duverger, E.; Sonnet, P.; Chaput, L.; Gourdon, A.; Cherioux, F. STM and DFT Investigations of Isolated Porphyrin on a Silicon-Based Semiconductor at Room Temperature. *ChemPhysChem* **2009**, *10*, 3190–3193. [[CrossRef](#)]
91. Boukari, K.; Sonnet, P.; Duverger, E. DFT-D Studies of Single Porphyrin Molecule on Doped Boron Silicon Surfaces. *ChemPhysChem* **2012**, *13*, 3945–3951. [[CrossRef](#)]
92. Chin, Y.; Panduwina, D.; Sintic, M.; Sum, T.J.; Hush, N.S.; Crossley, M.J.; Reimers, J.R. Atomic-Resolution Kinked Structure of an Alkylporphyrin on Highly Ordered Pyrolytic Graphite. *J. Phys. Chem. Lett.* **2011**, *2*, 62–66. [[CrossRef](#)]
93. Dapprich, S.; Komáromi, I.; Byun, K.S.; Morokuma, K.; Frisch, M.J. A new ONIOM implementation in Gaussian98. Part I. The calculation of energies, gradients, vibrational frequencies and electric field derivatives. Dedicated to Professor Keiji Morokuma in celebration of his 65th birthday. *J. Mol. Struct.* **1999**, *461*, 1–21. [[CrossRef](#)]
94. Reimers, J.R.; Panduwina, D.; Visser, J.; Chin, Y.; Tang, C.; Goerigk, L.; Ford, M.J.; Baker, M.; Sum, T.J.; Coenen, M.J.J.; et al. From Chaos to Order: Chain-Length Dependence of the Free Energy of Formation of Meso-tetraalkylporphyrin Self-Assembled Monolayer Polymorphs. *J. Phys. Chem. C* **2016**, *120*, 1739–1748. [[CrossRef](#)]
95. Fanetti, M.; Calzolari, A.; Vilmercati, P.; Castellarin-Cudia, C.; Borghetti, P.; Di Santo, G.; Floreano, L.; Verdini, A.; Cossaro, A.; Vobornik, I.; et al. Structure and Molecule–Substrate Interaction in a Co-octaethyl Porphyrin Monolayer on the Ag(110) Surface. *J. Phys. Chem. C* **2011**, *115*, 11560–11568. [[CrossRef](#)]
96. Chilukuri, B.; Mazur, U.; Hipps, K.W. Effect of dispersion on surface interactions of cobalt(II) octaethylporphyrin monolayer on Au(111) and HOPG(0001) substrates: A comparative first principles study. *Phys. Chem. Chem. Phys.* **2014**, *16*, 14096–14107. [[CrossRef](#)] [[PubMed](#)]
97. Kohn, W.; Sham, L.J. Self-Consistent Equations Including Exchange and Correlation Effects. *Phys. Rev.* **1965**, *140*, A1133–A1138. [[CrossRef](#)]
98. Tada, K.; Maeda, Y.; Ozaki, H.; Tanaka, S.; Yamazaki, S. Theoretical investigation on the interaction between Rh(III) octaethylporphyrin and a graphite basal surface: A comparison study of DFT, DFT-D, and AFM. *Phys. Chem. Chem. Phys.* **2018**, *20*, 20235–20246. [[CrossRef](#)] [[PubMed](#)]
99. Sena, A.M.P.; Brazdova, V.; Bowler, D.R. Density functional theory study of the iron-based porphyrin haem(b) on the Si(111):H surface. *Phys. Rev. B* **2009**, *79*, 245404/1–245404/7. [[CrossRef](#)]
100. Tersoff, J.; Hamann, D.R. Theory of the scanning tunneling microscope. *Phys. Rev. B* **1985**, *31*, 805–813. [[CrossRef](#)] [[PubMed](#)]
101. Hanke, F.; Haq, S.; Raval, R.; Persson, M. Heat-to-connect: Surface commensurability directs organometallic one-dimensional self-assembly. *ACS Nano* **2011**, *5*, 9093–9103. [[CrossRef](#)]

102. Dyer, M.S.; Robin, A.; Haq, S.; Raval, R.; Persson, M.; Klimeš, J. Understanding the Interaction of the Porphyrin Macrocycle to Reactive Metal Substrates: Structure, Bonding, and Adatom Capture. *ACS Nano* **2011**, *5*, 1831–1838. [[CrossRef](#)]
103. Miller, D.P.; Hooper, J.; Simpson, S.; Costa, P.S.; Tyminska, N.; McDonnell, S.M.; Bennett, J.A.; Enders, A.; Zurek, E. Electronic Structure of Iron Porphyrin Adsorbed to the Pt(111) Surface. *J. Phys. Chem. C* **2016**, *120*, 29173–29181. [[CrossRef](#)]
104. Leung, K.; Rempe, S.B.; Schultz, P.A.; Sproviero, E.M.; Batista, V.S.; Chandross, M.E.; Medforth, C.J. Density Functional Theory and DFT+U Study of Transition Metal Porphines Adsorbed on Au(111) Surfaces and Effects of Applied Electric Fields. *J. Am. Chem. Soc.* **2006**, *128*, 3659–3668. [[CrossRef](#)]
105. Berland, K.; Hyldgaard, P. Exchange functional that tests the robustness of the plasmon description of the van der Waals density functional. *Phys. Rev. B* **2014**, *89*, 035412. [[CrossRef](#)]
106. Nandi, G.; Chilukuri, B.; Hipps, K.W.; Mazur, U. Surface directed reversible imidazole ligation to nickel (II) octaethylporphyrin at the solution/solid interface: A single molecule level study. *Phys. Chem. Chem. Phys.* **2016**, *18*, 20819–20829. [[CrossRef](#)] [[PubMed](#)]
107. Gurdal, Y.; Hutter, J.; Iannuzzi, M. Insight into (Co)Porphyrin Adsorption on Au(111): Effects of Herringbone Reconstruction and Dynamics of Metalation. *J. Phys. Chem. C* **2017**, *121*, 11416–11427. [[CrossRef](#)]
108. Gurdal, Y. Theoretical investigation of metalated and unmetalated porphyrins immobilized on Ag(111) surface. *J. Incl. Phenom. Macrocycl. Chem.* **2019**, *95*, 273–283. [[CrossRef](#)]
109. Jahanbekam, A.; Chilukuri, B.; Mazur, U.; Hipps, K.W. Kinetically Trapped Two-Component Self-Assembled Adlayer. *J. Phys. Chem. C* **2015**, *119*, 25364–25376. [[CrossRef](#)]
110. Chilukuri, B.; Mazur, U.; Hipps, K.W. Cooperativity and coverage dependent molecular desorption in self-assembled monolayers: Computational case study with coronene on Au (111) and HOPG. *Phys. Chem. Chem. Phys.* **2019**, *21*, 10505–10513. [[CrossRef](#)]
111. Touzeau, J.; Barbault, F.; Maurel, F.; Seydou, M. Insights on porphyrin-functionalized graphene: Theoretical study of substituent and metal-center effects on adsorption. *Chem. Phys. Lett.* **2018**, *713*, 172–179. [[CrossRef](#)]
112. Zeng, J.; Chen, K. A nearly perfect spin filter and a spin logic gate based on a porphyrin/graphene hybrid material. *Phys. Chem. Chem. Phys.* **2018**, *20*, 3997–4004. [[CrossRef](#)]
113. Meir, Y.; Wingreen, N.S. Landauer formula for the current through an interacting electron region. *Phys. Rev. Lett* **1992**, *68*, 2512–2515. [[CrossRef](#)]
114. Zhao, J.; Ding, Y. Functionalization of Single-Walled Carbon Nanotubes with Metalloporphyrin Complexes: A Theoretical Study. *J. Phys. Chem. C* **2008**, *112*, 11130–11134. [[CrossRef](#)]
115. Correa, J.D.; Orellana, W. Optical response of carbon nanotubes functionalized with (free-base, Zn) porphyrins, and phthalocyanines: A DFT study. *Phys. Rev. B* **2012**, *86*, 125417. [[CrossRef](#)]
116. Ruiz-Tagle, I.; Orellana, W. Iron porphyrin attached to single-walled carbon nanotubes: Electronic and dynamical properties from ab-initio calculations. *Phys. Rev. B* **2010**, *82*, 115406. [[CrossRef](#)]
117. Zhao, J.; Ding, Y. Theoretical studies of chemical functionalization of the (8,0) boron nitride nanotube with various metalloporphyrin MP (M=Fe, Co, Ni, Cu, and Zn) complexes. *Mater. Chem. Phys.* **2009**, *116*, 21–27. [[CrossRef](#)]
118. Gomez, T.; Zarate, X.; Schott, E.; Arratia-Perez, R. Role of the main adsorption modes in the interaction of the dye [COOH-TPP-Zn(II)] on a periodic TiO₂ slab exposing a rutile (110) surface in a dye-sensitized solar cell. *RSC Adv.* **2014**, *4*, 9639–9646. [[CrossRef](#)]
119. Lin, Y.; Zhu, C.; Jiang, Z.; Zhao, Y.; Wang, Q.; Zhang, R.; Lin, S.H. Enhanced photovoltaic performance of dye-sensitized solar cells by the adsorption of Zn-porphyrin dye molecule on TiO₂ surfaces. *J. Alloy. Compd.* **2019**, *794*, 35–44. [[CrossRef](#)]
120. Lovat, G.; Forrer, D.; Abadia, M.; Dominguez, M.; Casarin, M.; Rogero, C.; Vittadini, A.; Floreano, L. Hydrogen capture by porphyrins at the TiO₂(110) surface. *Phys. Chem. Chem. Phys.* **2015**, *17*, 30119–30124. [[CrossRef](#)] [[PubMed](#)]
121. Wang, C.; Fan, Q.; Han, Y.; Martínez, J.I.; Martín-Gago, J.A.; Wang, W.; Ju, H.; Gottfried, J.M.; Zhu, J. Metalation of tetraphenylporphyrin with nickel on a TiO₂(110)-1 × 2 surface. *Nanoscale* **2015**, *8*, 1123–1132. [[CrossRef](#)]
122. Lewis, J.P.; Jelinek, P.; Ortega, J.; Demkov, A.A.; Trabada, D.G.; Haycock, B.; Wang, H.; Adams, G.; Tomfohr, J.K.; Abad, E.; et al. Advances and applications in the FIREBALL ab initio tight-binding molecular-dynamics formalism. *Phys. Status Solidi* **2011**, *248*, 1989–2007. [[CrossRef](#)]

123. Spoerke, E.D.; Small, L.J.; Foster, M.E.; Wheeler, J.; Ullman, A.M.; Stavila, V.; Rodriguez, M.; Allendorf, M.D. MOF-Sensitized Solar Cells Enabled by a Pillared Porphyrin Framework. *J. Phys. Chem. C* **2017**, *121*, 4816–4824. [[CrossRef](#)]
124. Xie, M.; Bai, F.; Wang, J.; Zheng, Y.; Lin, Z. Theoretical investigations on the unsymmetrical effect of β -link Zn-porphyrin sensitizers on the performance for dye-sensitized solar cells. *Phys. Chem. Chem. Phys.* **2018**, *20*, 3741–3751. [[CrossRef](#)]
125. Niskanen, M.; Kuisma, M.; Cramariuc, O.; Golovanov, V.; Hukka, T.I.; Tkachenko, N.; Rantala, T.T. Porphyrin adsorbed on the (1010) surface of the wurtzite structure of ZnO—conformation induced effects on the electron transfer characteristics. *Phys. Chem. Chem. Phys.* **2013**, *15*, 17408–17418. [[CrossRef](#)]
126. Torres, A.; Amaya Suarez, J.; Remesal, E.R.; Marquez, A.M.; Fernandez Sanz, J.; Rincon Canibano, C. Adsorption of Prototypical Asphaltenes on Silica: First-Principles DFT Simulations Including Dispersion Corrections. *J. Phys. Chem. B* **2017**. Ahead of Print. [[CrossRef](#)] [[PubMed](#)]
127. Quinn, T.; Choudhury, P. Direct oxidation of methane to methanol on single-site copper-oxo species of copper porphyrin functionalized graphene: A DFT study. *Mol. Catal.* **2017**, *431*, 9–14. [[CrossRef](#)]
128. Henkelman, G.; Uberuaga, B.P.; Jónsson, H. A climbing image nudged elastic band method for finding saddle points and minimum energy paths. *J. Chem. Phys.* **2000**, *113*, 9901–9904. [[CrossRef](#)]
129. Sheppard, D.; Terrell, R.; Henkelman, G. Optimization methods for finding minimum energy paths. *J. Chem. Phys.* **2008**, *128*, 134106. [[CrossRef](#)]
130. Henkelman, G.; Arnaldsson, A.; Jónsson, H. A fast and robust algorithm for Bader decomposition of charge density. *Comput. Mater. Sci.* **2006**, *36*, 354–360. [[CrossRef](#)]
131. Grill, L.; Dyer, M.; Lafferentz, L.; Persson, M.; Peters, M.V.; Hecht, S. Nano-architectures by covalent assembly of molecular building blocks. *Nat. Nanotechnol.* **2007**, *2*, 687–691. [[CrossRef](#)]
132. Shi, K.; Shu, C.; Wang, C.; Wu, X.; Tian, H.; Liu, P. On-Surface Heck Reaction of Aryl Bromides with Alkene on Au(111) with Palladium as Catalyst. *Org. Lett.* **2017**, *19*, 2801–2804. [[CrossRef](#)]
133. Shu, C.; Xie, Y.; Wang, A.; Shi, K.; Zhang, W.; Li, D.; Liu, P. On-surface reactions of aryl chloride and porphyrin macrocycles via merging two reactive sites into a single precursor. *Chem. Commun.* **2018**, *54*, 12626–12629. [[CrossRef](#)]
134. Wende, H.; Bernien, M.; Luo, J.; Sorg, C.; Ponpandian, N.; Kurde, J.; Miguel, J.; Piantek, M.; Xu, X.; Eckhold, P.; et al. Substrate-induced magnetic ordering and switching of iron porphyrin molecules. *Nat. Mater.* **2007**, *6*, 516–520. [[CrossRef](#)]
135. Oppeneer, P.M.; Panchmatia, P.M.; Sanyal, B.; Eriksson, O.; Ali, M.E. Nature of the magnetic interaction between Fe-porphyrin molecules and ferromagnetic surfaces. *Prog. Surf. Sci.* **2009**, *84*, 18–29. [[CrossRef](#)]
136. Weber, A.P.; Caruso, A.N.; Vescovo, E.; Ali, M.E.; Tarafder, K.; Janjua, S.Z.; Sadowski, J.T.; Oppeneer, P.M. Magnetic coupling of Fe-porphyrin molecules adsorbed on clean and c (2 × 2) oxygen-reconstructed Co(100) investigated by spin-polarized photoemission spectroscopy. *Phys. Rev. B* **2013**, *87*, 184411. [[CrossRef](#)]
137. Ali, M.E.; Sanyal, B.; Oppeneer, P.M. Tuning the Magnetic Interaction between Manganese Porphyrins and Ferromagnetic Co Substrate through Dedicated Control of the Adsorption. *J. Phys. Chem. C* **2009**, *113*, 14381–14383. [[CrossRef](#)]
138. Chylarecka, D.; Kim, T.K.; Tarafder, K.; Müller, K.; Gödel, K.; Czekaj, I.; Wäckerlin, C.; Cinchetti, M.; Ali, M.E.; Piamonteze, C.; et al. Indirect Magnetic Coupling of Manganese Porphyrin to a Ferromagnetic Cobalt Substrate. *J. Phys. Chem. C* **2011**, *115*, 1295–1301. [[CrossRef](#)]
139. Waeckerlin, C.; Maldonado, P.; Arnold, L.; Shchyrba, A.; Girovsky, J.; Nowakowski, J.; Ali, M.E.; Haehlen, T.; Baljovic, M.; Siewert, D.; et al. Magnetic exchange coupling of a synthetic Co(II)-complex to a ferromagnetic Ni substrate. *Chem. Commun.* **2013**, *49*, 10736–10738. [[CrossRef](#)]
140. Hermanns, C.F.; Tarafder, K.; Bernien, M.; Kruger, A.; Chang, Y.; Oppeneer, P.M.; Kuch, W. Magnetic coupling of porphyrin molecules through graphene. *Adv. Mater.* **2013**, *25*, 3473–3477. [[CrossRef](#)]
141. Lamoen, N.; Ballone, N.; Parrinello, N. Electronic structure, screening, and charging effects at a metal/organic tunneling junction: A first-principles study. *Phys. Rev. B* **1996**, *54*, 5097–5105. [[CrossRef](#)]
142. Picozzi, S.; Pecchia, A.; Gheorghe, M.; Di Carlo, A.; Lugli, P.; Delley, B.; Elstner, M. Organic/metal interfaces: An ab initio study of their structural and electronic properties. *Surf. Sci.* **2004**, *566*, 628–632. [[CrossRef](#)]
143. Long, M.; Chen, K.; Wang, L.; Qing, W.; Zou, B.S.; Shuai, Z. Negative differential resistance behaviors in porphyrin molecular junctions modulated with side groups. *Appl. Phys. Lett.* **2008**, *92*, 243303. [[CrossRef](#)]

144. An, Y.; Yang, Z.; Ratner, M.A. High-efficiency switching effect in porphyrin-ethyne-benzene conjugates. *J. Chem. Phys.* **2011**, *135*, 044706. [[CrossRef](#)]
145. Liu, Z.; Wei, S.; Yoon, H.; Adak, O.; Ponce, I.; Jiang, Y.; Jang, W.; Campos, L.M.; Venkataraman, L.; Neaton, J.B. Control of Single-Molecule Junction Conductance of Porphyrins via a Transition-Metal Center. *Nano Lett.* **2014**, *14*, 5365–5370. [[CrossRef](#)]
146. Stein, T.; Eisenberg, H.; Kronik, L.; Baer, R. Fundamental Gaps in Finite Systems from Eigenvalues of a Generalized Kohn-Sham Method. *Phys. Rev. Lett.* **2010**, *105*, 266802. [[CrossRef](#)] [[PubMed](#)]
147. Quek, S.Y.; Venkataraman, L.; Choi, H.J.; Louie, S.G.; Hybertsen, M.S.; Neaton, J.B. Amine–Gold Linked Single-Molecule Circuits: Experiment and Theory. *Nano Lett.* **2007**, *7*, 3477–3482. [[CrossRef](#)] [[PubMed](#)]
148. Quek, S.Y.; Choi, H.J.; Louie, S.G.; Neaton, J.B. Length Dependence of Conductance in Aromatic Single-Molecule Junctions. *Nano Lett.* **2009**, *9*, 3949–3953. [[CrossRef](#)] [[PubMed](#)]
149. Cho, W.J.; Cho, Y.; Min, S.K.; Kim, W.Y.; Kim, K.S. Chromium Porphyrin Arrays as Spintronic Devices. *J. Am. Chem. Soc.* **2011**, *133*, 9364–9369. [[CrossRef](#)]
150. Sedghi, G.; García-Suárez, V.M.; Esdaile, L.J.; Anderson, H.L.; Lambert, C.J.; Martín, S.; Bethell, D.; Higgins, S.J.; Elliott, M.; Bennett, N.; et al. Long-range electron tunnelling in oligo-porphyrin molecular wires. *Nat. Nanotechnol.* **2011**, *6*, 517–523. [[CrossRef](#)]
151. García-Suárez, V.M.; Ferradás, R.; Carrascal, D.; Ferrer, J. Universality in the low-voltage transport response of molecular wires physisorbed onto graphene electrodes. *Phys. Rev. B* **2013**, *87*. [[CrossRef](#)]
152. Sanders, J.K.; Bampos, N.; Clyde-Watson, Z.; Darling, S.L.; Hawley, J.C.; Kim, H.J.; Webb, S.J. Axial Coordination Chemistry of Metalloporphyrins. In *The Porphyrin Handbook*; Kadish, K.M., Smith, K.M., Guillard, R., Eds.; Academic: San Diego, CA, USA, 2000; pp. 1–48.
153. Gottfried, J.M. Surface chemistry of porphyrins and phthalocyanines. *Surf. Sci. Rep.* **2015**, *70*, 259–379. [[CrossRef](#)]
154. Gottfried, J.M.; Marbach, H. Surface-Confined Coordination Chemistry with Porphyrins and Phthalocyanines: Aspects of Formation, Electronic Structure, and Reactivity. *Zeitschrift Fur Physikalische Chemie-Int. J. Res. Phys. Chem. Chem. Phys.* **2009**, *223*, 53–74. [[CrossRef](#)]
155. Hieringer, W.; Flechtner, K.; Kretschmann, A.; Seufert, K.; Auwärter, W.; Barth, J.V.; Görling, A.; Steinrück, H.; Gottfried, J.M. The surface trans effect: Influence of axial ligands on the surface chemical bonds of adsorbed metalloporphyrins. *J. Am. Chem. Soc.* **2011**, *133*, 6206–6222. [[CrossRef](#)]
156. Seufert, K.; Auwärter, W.; Barth, J.V. Discriminative Response of Surface-Confined Metalloporphyrin Molecules to Carbon and Nitrogen Monoxide. *J. Am. Chem. Soc.* **2010**, *132*, 18141–18146. [[CrossRef](#)]
157. Friesen, B.A.; Bhattarai, A.; Mazur, U.; Hipps, K.W. Single Molecule Imaging of Oxygenation of Cobalt Octaethylporphyrin at the Solution/Solid Interface: Thermodynamics from Microscopy. *J. Am. Chem. Soc.* **2012**, *134*, 14897–14904. [[CrossRef](#)] [[PubMed](#)]
158. Wäckerlin, C.; Tarafder, K.; Siewert, D.; Girovsky, J.; Hählen, T.; Iacovita, C.; Kleibert, A.; Nolting, F.; Jung, T.A.; Oppeneer, P.M.; et al. On-surface coordination chemistry of planar molecular spin systems: Novel magnetochemical effects induced by axial ligands. *Chem. Sci.* **2012**, *3*, 3154–3160. [[CrossRef](#)]
159. Janet, J.P.; Zhao, Q.; Ioannidis, E.I.; Kulik, H.J. Density functional theory for modelling large molecular adsorbate–surface interactions: A mini-review and worked example. *Mol. Simul.* **2017**, *43*, 327–345. [[CrossRef](#)]
160. Ghosh, D.; Parida, P.; Pati, S.K. Spin-state switching of manganese porphyrin by conformational modification. *J. Phys. Chem. C* **2016**, *120*, 3625–3634. [[CrossRef](#)]
161. Nguyen, T.Q.; Aspera, S.M.; Nakanishi, H.; Kasai, H. NO adsorption effects on various functional molecular nanowires. *Comput. Mater. Sci.* **2009**, *47*, 111–120. [[CrossRef](#)]
162. Nguyen, T.Q.; Escaño, M.C.S.; Shimoji, N.; Nakanishi, H.; Kasai, H. Adsorption of diatomic molecules on iron tape-porphyrin: A comparative study. *Phys. Rev. B* **2008**, *77*, 195307. [[CrossRef](#)]
163. Nguyen, T.Q.; Escaño, M.C.S.; Shimoji, N.; Nakanishi, H.; Kasai, H. DFT study on the adsorption of NO on iron tape-porphyrin. *Surf. Interface Anal.* **2008**, *40*, 1082–1084. [[CrossRef](#)]

